University of Nevada, Reno

# Electrostimulation of $Ca^{2+}$ influx into adrenal chromaffin cells by nanoelectropulses: The impact of increasing pulse duration from 3 to 50 ns on $Ca^{2+}$ entry pathways

A thesis submitted in partial fulfillment of the

requirements for the degree of Master of Science in

Biomedical Engineering

By

Sung-Hae Yun

Dr. Josette El Zaklit / Thesis Advisor

Dr. Ji Hwan Yoon / Thesis Co-Advisor

December, 2022

THE GRADUATE SCHOOL

We recommend that the thesis
prepared under our supervision by

**Sung-Hae Yun**

Entitled

**Electrostimulation of $Ca^{2+}$ influx into adrenal chromaffin cells by nanoelectropulses: The impact of increasing pulse duration from 3 to 50 ns on $Ca^{2+}$ entry pathways**

be accepted in partial fulfillment of the
requirements for the degree of

MASTER OF SCIENCE

Josette El Zaklit, Ph.D., *Advisor*

Ji Hwan Yoon, Ph.D., *Co-Advisor*

Gale L. Craviso, Ph.D., *Committee Member*

Thomas Gould, Ph.D., *Graduate School Representative*

Markus Kemmelmeier, *Dean, Graduate School*

December, 2022

## ABSTRACT

Electrostimulation is commonly used in clinical applications to treat neurological diseases and disorders. It can be achieved invasively by implanted electrodes such as in deep brain stimulation, or non-invasively such as in transcranial direct current stimulation where electrodes are placed on the scalp. Here, we propose a novel electrical stimulus, high intensity nanosecond duration electric pulses (NEPs) for their capability to target deep areas in the body non-invasively, without the use of implanted electrodes. However, before developing neuromodulation technologies based on this novel stimulus, it is imperative to understand how NEPs interact with neural cell types and identify the range of NEP parameters that trigger cell excitation in the absence of adverse effects. In this study, we used isolated bovine adrenal chromaffin cells, a well-characterized neural-type cell, as our cell model to investigate how NEPs that are 3 to 50 ns in duration affect chromaffin cell excitability.

We have previously shown that in bovine adrenal chromaffin cells loaded with a fluorescent $Ca^{2+}$ indicator, a single 5 ns electric pulse, similar to the physiological stimulus, causes an immediate rise in intracellular $Ca^{2+}$ level ($[Ca^{2+}]_i$) that is solely due to $Ca^{2+}$ influx via voltage-gated $Ca^{2+}$ channels (VGCCs). However, when the electric pulse duration is increased to 150 ns, it causes $Ca^{2+}$ influx into cells by at least two pathways. One is VGCCs (60-70%), and another via a plasma membrane pathway(s) (30-40%) that is yet to be identified. Thus, the main goal of this study was to identify the pulse duration at which $Ca^{2+}$ influx begins to involve a non-VGCC pathway. To achieve our goal, we used two

variable duration pulse generators, one with a pulse duration ranging from 3 to 11 ns, and another with a pulse duration ranging from 12 to 100 ns.

First, we found that applying NEPs ranging from 3 to 50 ns in duration at their respective threshold electric fields caused a rapid rise in $[Ca^{2+}]_i$ that increased in duration and magnitude as pulse duration was increased. Two patterns of responses were observed. For pulse durations less than 11 ns, $Ca^{2+}$ responses were mainly transient (i.e. returned to baseline within 30 s following pulse application) in the majority (~75%) of the cells. However, when the pulse duration was increased to 11 ns, the majority (~77%) of the cells exhibited longer-lived $Ca^{2+}$ responses, and by 50 ns, 100% of the cells had longer-lived activity. To determine if $Ca^{2+}$ release from intracellular stores contributed to the longer-lived $Ca^{2+}$ responses, we conducted experiments in the absence of external $Ca^{2+}$. We found that none of the cells exhibited $Ca^{2+}$ responses without extracellular $Ca^{2+}$ indicating that the $Ca^{2+}$ responses observed were solely due to $Ca^{2+}$ influx into cells.

Therefore, to identify the pathway for $Ca^{2+}$ entry, VGCCs were blocked with a cocktail of inhibitors containing 100 nM ω-agatoxin IVA, 20 nM ω-conotoxin GVIA, and 20 μM nitrendipine to block P/Q-, N-, and L-type VGCCs, respectively. We found that $Ca^{2+}$ responses evoked by 3 and 5 ns pulses were fully abolished, while those evoked by 11 were significantly attenuated relative to the control. Increasing pulse duration to 50 ns reduced $Ca^{2+}$ entry into cells by about 50%, indicating that 50% of the $Ca^{2+}$ responses were due to a non-VGCC entry pathway. In the next series of experiments, cells were treated with $Cd^{2+}$, an inorganic, non-selective blocker of VGCCs. Similar to what we have found with a 150

ns pulse, all $Ca^{2+}$ responses evoked by 11 and 50 ns durations were completely eliminated, indicating that $Cd^{2+}$ blocked all $Ca^{2+}$ entry pathways into cells.

Because bipolar NEPs are known to reduced unwanted cellular membrane effects, we next determined if changing the shape of the 11 ns pulse, which is the pulse duration at which the cell membrane starts to involve a non-VGCC $Ca^{2+}$ entry pathway, would reduce/eliminate the additional $Ca^{2+}$ entry pathway. We found that application of a 11 ns bipolar pulse in which a positive pulse was immediately followed by a negative pulse of opposite polarity abolished $Ca^{2+}$ responses in about 70% of the cells, with the remaining 30% exhibiting transient $Ca^{2+}$ responses. Interestingly, blocking VGCCs with a cocktail of blockers caused $Ca^{2+}$ responses to be totally eliminated in all cells tested, indicating that, unlike a 11 ns unipolar pulse, a 11 ns bipolar pulse caused $Ca^{2+}$ influx into cells that was solely due to VGCCs, thus eliminating the additional pathway of $Ca^{2+}$ entry into cells.

Lastly, we investigated the $Na^{+}$ dependency on the $Ca^{2+}$ responses when cells were subjected to pulses that were 3, 5, 11 and 50 ns in duration. For this investigation, NEPs were applied to cells in $Na^{+}$-free medium where either $TMA^{+}$ or $NMDG^{+}$ was used as a substitute for $Na^{+}$. In both $TMA^{+}$- and $NMDG^{+}$-containing solutions, we found that for pulse durations less than 11 ns, the pulse-induced rise in $[Ca^{2+}]_i$ was almost fully abolished, indicating that $Na^{+}$ was necessary to evoke the pulse-induced $Ca^{2+}$ rise. For the longer duration pulses (i.e. > 11 ns), the pulse-induced rise in $[Ca^{2+}]_i$ was significantly attenuated in $Na^{+}$-free solution relative to the control. These results indicate that for pulses shorter than 11 ns, $Na^{+}$ entry played a role in the mechanism by which NEPs evoked $Ca^{2+}$ influx, whereas, for pulses longer than 11 ns, there remains an NEP-induced $Ca^{2+}$ influx pathway

that was not dependent on external $Na^+$. Of note is that, similar to what we previously found with 5 ns pulses, $Na^+$ entry did not occur via voltage-gated $Na^+$ channels since the $Na^+$ channel blocker tetrodotoxin (TTX) failed to block the NEP-induced rise in $[Ca^{2+}]_i$ for all pulse durations.

Taken together, these results indicate that a single ultrashort (< 11 ns) electric pulse causes $Ca^{2+}$ influx solely via VGCCs in a manner involving $Na^+$ influx, while longer-duration pulses cause $Ca^{2+}$ influx not only via VGCCs but also via a non-VGCC pathway that is yet to be identified. These results highlight the sensitivity of excitable adrenal chromaffin cells to ultrashort pulse durations that differ by only tens of nanoseconds, which is important for the development of future technologies aimed at using NEPs for neuromodulation.

## DEDICATION

To my dearest Goomi for staying by my side for countless nights in the lab, Jeong-Hwan for sharing his witty wisdom every time I needed a lift from the slump. And to the Yoon family, Raymond, my parents, my friends Ponderosa, and Narmeen, who encouraged and supported me in every possible way they could.

## ACKNOWLEDGEMENTS

I acknowledge all the people in our research group who have helped me, each in their own way. I profoundly thank Dr. Josette El Zaklit for being an amazing advisor and trusting me with my ability and potential. I thank Dr. Jihwan Yoon for being my mentor and encouraging me to become an accountable person to myself. I thank my colleagues Vasilii Mansurov and Farhana Hossain for all the support and friendship that we shared to get through the program. I thank Dr. Lisha Yang, Anitha Balaji and Kyung Eun You for preparing bovine adrenal chromaffin cells. I thank all the undergraduate students for volunteering in our lab and sharing positive energy.

This work was supported by the Air Force Office of Scientific Research (AFOSR) Grants FA9550-14-1-0018, FA9550-20-1-0061, and MURI FA9550-15-1-0517, and the National Institute of General Medical Sciences of the National Institutes of Health under grant number P20 GM103650.

# CONTENTS

# LIST OF TABLES

# LIST OF FIGURES

# LIST OF ABBREVIATIONS

| | |
|---|---|
| ES | Electrostimulation |
| E-field | Electric field |
| NEP(s) | Nanosecond electric pulse(s) |
| NEpi | Norepinephrine |
| Epi | Epinephrine |
| ACh | Acetylcholine |
| nAChR | Nicotinic acetylcholine receptor |
| VGCC(s) | Voltage-gated $Ca^{2+}$ channel(s) |
| VGSC(s) | Voltage-gated $Na^{+}$ channel(s) |
| $[Ca^{2+}]_i$ | Intracellular calcium levels |
| TIRFM | Total internal reflection fluorescence microscopy |
| $V_{max}$ | Measured voltage amplitude |
| FWHM | Measured full width at half maximum |
| DMPP | 1,1-dimethyl-4-phenylpiperazinium |
| TMP | Transmembrane potential |
| FITC | Fluorescein isothiocyanate |
| HBSS | Hank's balanced salt solution |
| BSA | Bovine serum albumin |
| BSS | Balanced salt solution |
| EGTA | Ethylene glycol-bis(β-aminoethyl ether)-N,N,N',N'-tetraacetic acid |
| $TMA^{+}$ | tetramethylammonium hydroxide |

| | |
|---|---|
| $NMDG^+$ | *N*-methyl-D-glucamine |
| TTX | tetrodotoxin |
| LAS X | Leica Application Suite X |
| ROI(s) | Region of interest(s) |
| SEM | Standard error mean |

# Chapter 1. INTRODUCTION

## 1.1 Electrostimulation for neuromodulation

Electrical stimulation (ES) is widely used for treating neurological and psychiatric diseases and disorders such as dystonia, Parkinson's disease, and obsessive-compulsive disorder (Perlmutter et al., 2006). ES involves the use of implanted electrodes or non-implanted electrodes placed on the scalp. For example, in deep brain stimulation, surgically-implanted electrodes deliver microsecond-duration electric pulses into targeted areas deep inside the brain. Non-invasive techniques such as transcranial direct current stimulation are achieved without surgery with electrodes placed on the surface of the head. Yet, the latter application does not offer enough focused ES due to the size of the electrodes. Thus, researchers are always working on developing safer and better targeted ES technologies for neuromodulation.

## 1.2 Nanosecond-duration electric pulses can serve as a novel non-invasive and efficient neurostimulation modality

Advances in pulsed power technologies have produced a new type of bioelectric stimulus, nanosecond-duration electric pulses (NEPs), that have the potential to achieve non-invasive and targeted stimulation via antennas, which could eliminate the need for invasive electrodes (Petrella et al.,2016). In addition, due to their high-frequency content and ultrashort duration, NEPs offer the opportunity to transfer electrical energy to a small, focused area deep into biological tissues. Another feature of NEPs is that they can cancel

a stimulatory effect such as $Ca^{2+}$ influx into neural-type cells, by applying a second pulse of opposite polarity, a phenomenon called bipolar cancellation (Gianulis et al., 2019). A possible application of bipolar cancellation is remote stimulation by a "cancellation of cancellation" or CANCAN effect. In theory, the CANCAN effect could be optimized to achieve intense focusing of NEPs to a small area in a tissue by using two or more pairs of electrodes. As a potentially important functional consequence, CANCAN could provide new means to alter cell excitability, thereby serving as a safe technology to achieve focused electric stimulation for neuromodulation.

NEPs have been shown to stimulate intact nerves (Casciola et al., 2017), nociceptors (Jiang & Cooper., 2011), hippocampal neurons (Roth et al., 2013), and as our studies have shown, excitable neuroendocrine adrenal chromaffin cells (Vernier et al., 2008; Craviso et al., 2009; Craviso et al., 2010; and Craviso et al.,2012).

## 1.3 Adrenal chromaffin cells, a model of neurosecretion

### 1.3.1 Biology of chromaffin cells

Adrenal chromaffin cells are neuroendocrine cells that are found in the medulla of adrenal glands, which are located on top of the kidneys. They are best known as the cell type that mediates the "fight or flight" response by releasing the catecholamines norepinephrine (NEpi) and epinephrine (Epi) together with neuropeptides into the bloodstream. A single chromaffin cell contains a large number of secretory granules that contain these catecholamines and occupy about 30% of the volume of the cell. Chromaffin cells are derived from the neural crest and share many similarities with sympathetic

neurons. Mainly, the release of catecholamines occurs by exocytosis through the same $Ca^{2+}$-dependent mechanism used by neurons to release neurotransmitters at nerve terminals. For these reasons, isolated chromaffin cells are an ideal neural-type model to be used to characterize mechanisms underlying stimulus-secretion coupling.

### 1.3.2 **Physiological stimulus for evoking catecholamine release *in vivo***

Chromaffin cells are innervated by the splanchnic nerve originating in the spinal cord. The sympathetic nerves tonically release acetylcholine (ACh) that binds to and activates nicotinic acetylcholine receptors (nAChR) on the membrane of chromaffin cells. These receptors are ligand-gated, non-selective cation channels permeable to $Na^+$ and $Ca^{2+}$. Upon activation, nAChRs allow $Na^+$ to enter the cell causing membrane depolarization, voltage-gated $Ca^{2+}$ channel (VGCC), activation, $Ca^{2+}$ influx, and the exocytotic release of catecholamines (Figure 1.1). During stress, ACh release increases, causing a surge of catecholamines into the bloodstream that triggers the “fight-or-flight” response.

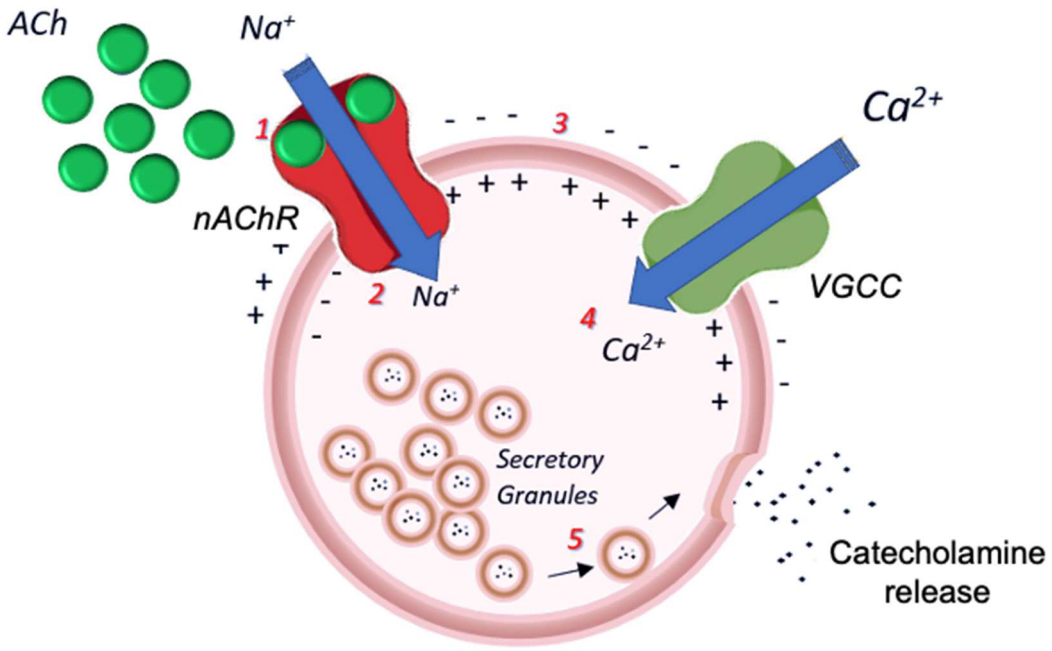


**Figure 1.1 Schematic of $Ca^{2+}$-mediated exocytosis in chromaffin cells *in vivo.*** 1) ACh binding to the nAChR, 2) $Na^+$ influx into the cytoplasm, 3) membrane depolarization, 4) $Ca^{2+}$ influx through VGCCs, 5) $Ca^{2+}$-dependent granule fusion causing exocytosis and secretion of catecholamines.

### 1.3.3 Effects of NEPs on bovine adrenal chromaffin cells

In recent decades, our group has been investigating the effect of NEPs on adrenal chromaffin cells. The major finding is that a single 5 ns, 5 MV/m electric pulse is sufficient to cause $Ca^{2+}$ influx solely via VGCCs and the subsequent release of catecholamines (Craviso et al., 2009; 2010). The mechanism responsible for VGCC activation and hence $Ca^{2+}$ influx is consistent with $Na^+$-dependent membrane depolarization mediated by either reversible permeabilization of the cell membrane to $Na^+$ (Craviso et al., 2009, Yoon et al., 2016) or $Na^+$ entry via non-selective protein ion channels ( Yang et al., 2021). Recently, we reported that a single 2 ns pulse, similar to a 5 ns pulse,

causes $Ca^{2+}$ influx via VGCCs (Zaklit et al., 2021). However, a longer duration pulse (150 ns), delivered at just above the threshold E-field, elicited $Ca^{2+}$ entry not only via VGCCs but also via another plasma membrane pathway that remains to be identified (Bagalkot et al., 2018). Figure 1.2 shows a schematic of the responses activated by NEPs applied to a chromaffin cell.

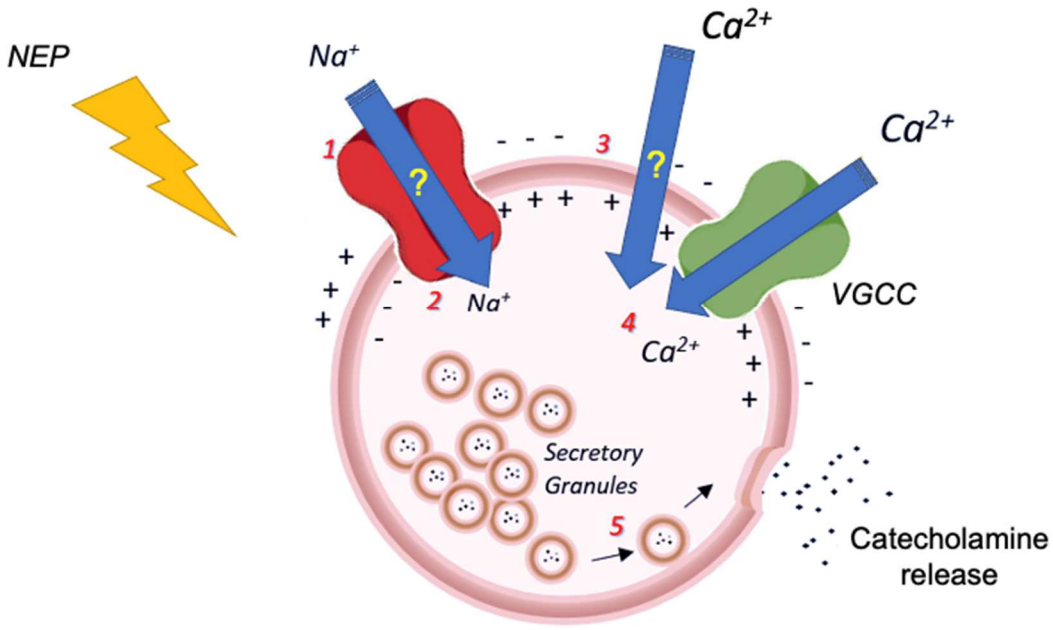


**Figure 1.2 Schematic of the stimulation of chromaffin cells by NEPs.** Application of a single 5 ns pulse causes 1) $Na^+$ to enter the cell through an unidentified pathway, which causes 2) membrane depolarization. This causes 3) the opening of VGCCs and $Ca^{2+}$ influx, and 4) subsequent release of catecholamines. However, a 150 ns pulse causes an additional $Ca^{2+}$ entry pathway, as indicated by the question mark on the blue arrow.

## 1.4 Objectives of this study

As mentioned earlier, our group found that a single 5 ns pulse delivered just above the threshold electric (E)-field, triggers a rise in intracellular $Ca^{2+}$ level ($[Ca^{2+}]_i$) that

involves $Ca^{2+}$ influx primarily via voltage-gated calcium channels (VGCCs) (Craviso et al. 2010). This VGCC-mediated influx of $Ca^{2+}$ entry is desirable since it mimics that evoked by the physiological stimulus. However, Bagalkot et al. (2018) recently reported that a longer duration 150 ns pulse delivered at just above the threshold E-field, elicited $Ca^{2+}$ influx not only via VGCCs but also via a non-VGCC pathway. By having the dual pathway of $Ca^{2+}$ entry, the cells exhibited greater $Ca^{2+}$ amplitudes and much longer-lived $Ca^{2+}$ responses despite the much lower E-field amplitude applied (0.31 MV/m for a 150 ns pulse compared to 3-4 MV/m for a 5 ns pulse) Thus, changing pulse duration appears to have a bigger effect on the response of the cells than changing the amplitude of the pulse.

Thus, the first goal of this study was to identify the optimal range of pulse durations to stimulate adrenal chromaffin cells in a way that resembles the physiological stimulus, i.e., identify the pulse duration at which the cell responses begin to include a non-VGCC pathway. The second goal was to characterize the plasma membrane changes accompanying this other $Ca^{2+}$ entry pathway.

Chapter 1 in this work provides an Introduction to the project and what is known about NEP stimulation of isolated adrenal chromaffin cells. Chapter 2 is a detailed description of the Methods used. The Results and Discussion of the experiments are presented in Chapter 3. Chapter 4 presents the Conclusion and Future Work.

# Chapter 2. MATERIALS AND METHODS

This project used wide-field epifluorescence microscopy to monitor NEP-induced $[Ca^{2+}]_i$ rises using cells loaded with the fluorescent $Ca^{2+}$ indicator Calcium Green-1. This chapter provides details on how bovine chromaffin cells were isolated from the adrenal gland and prepared for experiments. The details on what procedure was used to label the cell with the Calcium Green-1 dye and how to pretreat the cells with toxins and blockers are described as well as how the data analysis was done. A detailed description of the NEP exposure system used to deliver pulses and the parameters to image the cell responses are also described.

## 2.1 Chromaffin cell culturing and dissociation

From Wolf Pack Meats, Reno, NV, we were provided with fresh adrenal glands that we used to prepare adrenal chromaffin cells. Briefly, after the inner medullas of the adrenal glands were dissected from the cortex, a perfusion catheter was placed into the adreno-lumbar vein. Using $Ca^{2+}$/$Mg^{2+}$-free Hank's Balanced Salt Solution (HBSS) of the following composition: 137 mM NaCl, 5.37 mM KCl, 0.44 mM $KH_2PO_4$, 0.54 mM $Na_2HPO_4$, 4.17 mM $NaHCO_3$, 5.55 mM D-glucose, 5 mM HEPES, 0.001% phenol red and 0.02% bovine serum albumin (BSA), pH 7.2, the tissue was perfused for 5 min to flush away red blood cells. Next, the medulla was digested by perfusing with HBSS containing 0.05% of collagenase B and 50 μM $CaCl_2$. This process was done for 30 to 45 minutes at 27 to 30 °C. The swollen medulla was then transferred into a glass beaker containing HBSS

lacking collagenase. The digested tissue was then gently agitated against the walls of the beaker to break it down. The resulting cell suspension was filtered through a nylon mesh to remove tissue debris. The cell solution was then subjected to four centrifugation steps to separate chromaffin cells from any remaining red blood cells and debris. After the final centrifugation step, the cells were diluted in Ham's F-12 medium containing 10% bovine calf serum, 100 U/ml penicillin, 100 μg/ml streptomycin, 0.25 μg/ml fungizone, and 6 μg/ml cytosine arabinoside. After dilution, cells were placed into vented tissue culture flasks at an estimated concentration of 4 x $10^5$ cells/ml and incubated at 36.5 ℃ under a humidified atmosphere of 5% $CO_2$ for 5.5 hours. This step allowed non-chromaffin cells to adhere to the bottom of the flasks whereas chromaffin cells stayed in suspension. At the end of the differential plating step, the cells were collected from each flask, distributed into 60 mm Petri dishes at a density of 1 x $10^5$ cells/ml and maintained in suspension culture in the supplemented Hams' F12 medium at 36.5°C under a humidified atmosphere of 5% $CO_2$. Cells were used up until 2 weeks in culture.

## 2.2 Chromaffin cell dissociation and preparation for experiments

Chromaffin cells form large aggregates when they are in suspension culture. Thus, prior to conducting an experiment, dissociation has been done to dissociate the large clusters of cells into single cells. This process was done with the protease dispase as previously described (Craviso, 2004). Protease dispase II (~ 18 U/ml) and 0.2M of $CaCl_2$ were added to the 60-mm dish of cells maintained in suspension culture. The cells were incubated with the enzyme for at least 6 hours and no longer than 15 hours at 37°C with a

humidified atmosphere of 5% $CO_2$. After incubation, the cells were transferred into a 15-ml conical tube and centrifuged at 30 x g for 10 minutes at room temperature. After centrifugation, only the cell pellet was collected and resuspended in $Ca^{2+}$/$Mg^{2+}$-free HBSS of the following composition: 145 mM NaCl, 5 mM KCl, 1.2 mM $Na_2HPO_4$, 10 mM D-Glucose, 15 mM HEPES, pH 7.4. The cells in $Ca^{2+}$/$Mg^{2+}$-free HBSS were then incubated at 36.5 °C for 10 minutes in the water bath. The incubation was interrupted every 10 minutes to gently triturate 7-10 times with a 5-ml plastic pasture pipette for the aggregated cells to facilitate dissociation. The process of trituration and incubation was repeated 2 to 3 times until the dissociation was complete, making the whole process 30 to 40 minutes in total. The level of dissociation can be checked with the microscope for each titration between the 10-minute incubation periods. In the end, the cell aggregates were fully dissociated into single cells or small clusters of 2 to 3 cells. Then once again, the cell-containing tube was centrifuged at 67 x g for 10 minutes at room temperature. After that, the pellet of cells was collected and gently titrated with approximately 800 µl of pre-incubated Ham's F-12 medium containing Ara-C using a positive displacement pipette. Next, cells were placed onto fibronectin-coated 35-mm glass-bottom dishes. Dishes of attached cells were kept in the incubator at 36.5 ℃ under a humidified atmosphere of 5% $CO_2$ and cells were used from 1 to 2 days after attachment.

## 2.3 Fluorescence imaging of $[Ca^{2+}]_i$

### 2.3.1 Preparing the cells for imaging

For $Ca^{2+}$ imaging experiments, attached cells were washed with balanced salt solution (BSS) of the following composition: 145 mM NaCl, 5 mM KCl, 1.2 mM $NaH_2PO_4$, 2 mM $CaCl_2$, 1.3 mM $MgCl_2$, 10 mM glucose, 15 mM HEPES with a pH of 7.4. Then cells were incubated with 1 μM of the cell-permeant $Ca^{2+}$-sensitive fluorescent indicator Calcium Green-1, AM ($\lambda_{exc.}$ = 506 nm, $\lambda_{em.}$ = 531 nm) in BSS with 0.1% BSA for 45 minutes at 37 ℃. At the end of the incubation, cells were washed twice with dye-free BSS without BSA.

### 2.3.2 Imaging setup and analysis

Calcium Green-1 loaded cells were placed on the stage of an inverted DMi8 epifluorescence microscope (Leica Microsystems, Inc.) equipped with an electron-multiplying CCD iXon Ultra 897 (Andor) camera. A Leica Application Suite X (LAS X) software was used to automatically control all the imaging parameters. All the experiments were performed at ambient room temperature using a 63X dry objective.

The fluorophore was excited with a blue light ($\lambda_{exc.}$= 488 nm) illuminated by a Lambda DG4 Plus light source (Sutter Instruments). A FITC filter block with green emission was used to detect the emitted light. $Ca^{2+}$ imaging sequences were captured at a frame rate of ~7 frames/s, which is 150 ms of exposure time. The bright field images of each cell before and after applying the pulse were captured with an exposure time of 25

ms. Acquired sequences of the cells before, during, and after NEP application were analyzed using LAS X software. The region of interest (ROI) was drawn over the whole cell that was exposed to a NEP. For all the images, cell-free background fluorescence intensity was subtracted from the fluorescence intensity of the cells ($F = F_{cell} - F_{background}$). The fluorescence intensity $F$ was then normalized to the intensity value measured when the stimulus was applied ($F_0$) using a customized MATLAB program to get the final plot showing the fluorescence of $F/F_0$ for each cell. Figure 2.1A shows how the target cell with electrodes was positioned. Figure 2.1B shows how ROIs were set to obtain the fluorescence intensity of the cells.

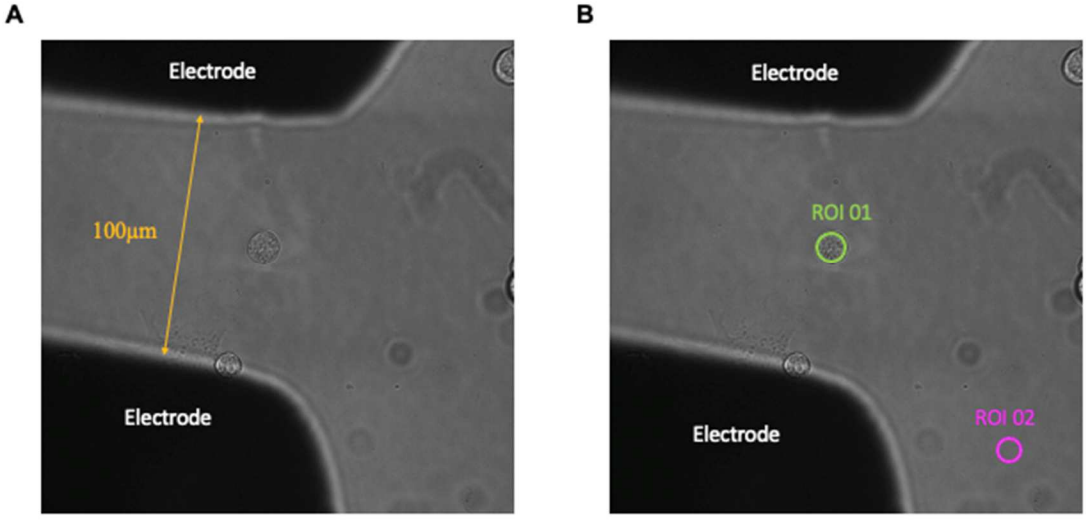


**Figure 2.1 Cell positioning between the electrode tips.** (A) Bright-field image of a cell positioned in between the electrode tips of the two cylindrical tungsten rod electrodes spaced 100 µm apart with the target cell in between them. (B) Same as (A) but with the green and purple circles indicating the regions of interest of the cell (ROI 01) and the back ground (ROI 02) used in the image analysis.

### 2.3.3 **Pretreating cells with voltage-gated $Ca^{2+}$ and $Na^{+}$ blockers**

For the experiments in which VGCCs blockers were used, cells were incubated for 60 min at 37 °C with a cocktail of toxins that include 100 nM ω-agatoxin IVA, 20 nM ω-conotoxin GVIA, and 20 μM nitrendipine to block P/Q-, N-, and L-type VGCCs, respectively. For experiments in which VGCCs were blocked with the inorganic, non-selective blocker $CdCl_2$, cells were incubated for 30 min at 37 °C with 200 μM $Cd^{2+}$ in BSS. For experiments in which voltage-gated $Na^{+}$ channels (VGSCs) were blocked, cells were incubated for 20 min at room temperature with 10 μM tetrodotoxin (TTX) which is a specific blocker for VGSCs.

### 2.3.4 **Conducting experiments under $Ca^{2+}$-free and $Na^{+}$ -free conditions**

For experiments carried out under $Ca^{2+}$-free conditions, the BSS contained 1 mM ethylene glycol-bis (β-aminoethyl ether)-N,N,N',N'-tetraacetic acid (EGTA). The dye-loaded cells were washed twice with $Ca^{2+}$-free BSS with EGTA before imaging.

For experiments conducted in the absence of external $Na^{+}$, $Na^{+}$ in the external solution was replaced with an equimolar concentration of tetramethylammonium hydroxide (TMA-OH, which we will refer to as $TMA^{+}$) to maintain isotonicity. The osmolarity and conductivity of the $TMA^{+}$ solution were close to that of BSS (314.6 ± 0.3 mOsm and 298.3 ± 1.2 mOsm, for the osmolarities of BSS and $TMA^{+}$, respectively; and 17.3 ± 0.2 mS/cm and 14.9 ± 0.5 mS/cm, for the conductivities of BSS and $TMA^{+}$, respectively). For experiments conducted in the absence of external $Na^{+}$, $Na^{+}$ was replaced with an equimolar concentration of *N*-methyl-D-glucamine ($NMDG^{+}$).

## 2.4 NEP exposure

Pulses 3 to 50 ns in duration were generated by two variable amplitude (± 1-5 kV), variable duration, nanosecond bipolar pulse generators, FPG 5-1NL10V2 and FPG 5-01NL100V2 (FID GmbH, Germany). The shorter-duration pulser delivers pulses 3 to 11 ns in duration, while the longer-duration pulser delivers pulses 12 to 100 ns in duration. The 3 and 5 ns pulses obtained from the shorter-duration pulse generator have a bell-shaped curve with a full-width at half maximum (FWHM) of 3.6 and 5.4 ns, and a rise time (measured from 10% to 90% of the pulse peak) of 2.0 and 2.4 ns, respectively. The 11 ns pulse duration obtained from the short-duration pulser has a trapezoidal shape with a FWHM of 11.4 and a rise time of 4.2 ns, while the 12 ns pulse duration obtained from the longer-duration pulse generator has a bell-shaped curve with a full FWHM of 12.4 ns, and a rise time of 5.1 ns. For experiments using 11 ns pulses, the shorter-duration pulse generator was used. The 50 ns pulse has a trapezoidal shape with a FWHM of 49.4 ns and rise time of 6.5 ns.

Pulses were applied via a pair of custom-made tungsten rod electrodes (127 μm diameter obtained from A-M Systems, Sequim, WA) soldered to a BNC connector. Figure 2.2 shows the electrodes used to deliver the pulses to cells. The tips of the tungsten electrodes were separated by a 100 μm gap and positioned 40 μm above the bottom of the dish using a micromanipulator (MP 224, Sutter Instruments), with the cell positioned in between the electrode tips as shown in Figure 2.2.

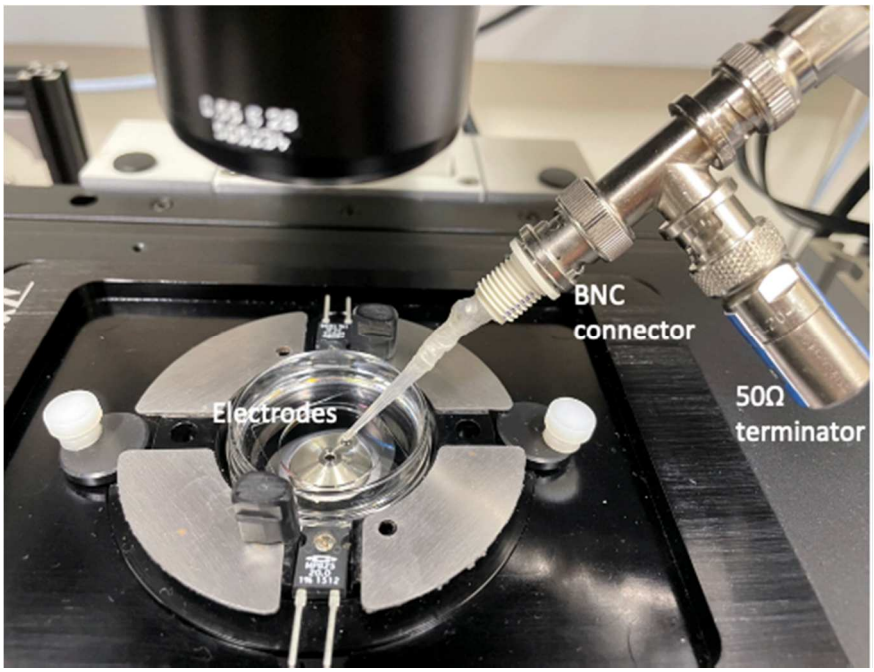


**Figure 2.2 Photograph of the electrodes used to deliver NEPs to cells.** Shown is a close-up view of the electrodes soldered to a BNC connector immersed in the BSS in the glass-bottom dish where bovine chromaffin cells are attached. A 50 Ω terminator is placed at the T-connection.

Figure 2.3 shows the NEP exposure setup. The pulsers were triggered externally by a custom program written in LabVIEW, and the camera was synchronized with the pulse generator to precisely determine the time at which the pulses were applied to the cells. Depending on pulse duration, pulses were delivered to the electrodes at amplitudes that produced E-fields ranging from 1.1 to 13.4 MV/m at the location of the cell. The E-field distribution in the vicinity and at the location of the target cell was computed using the commercially available Finite-Difference Time-Domain (FDTD) software package SEMCAD X (version 14.8.5, SPEAG, Zurich, Switzerland) as previously described (Zaklit et al. 2017). Pulse traces were captured with an oscilloscope. Each cell was exposed only once to the applied E-field.

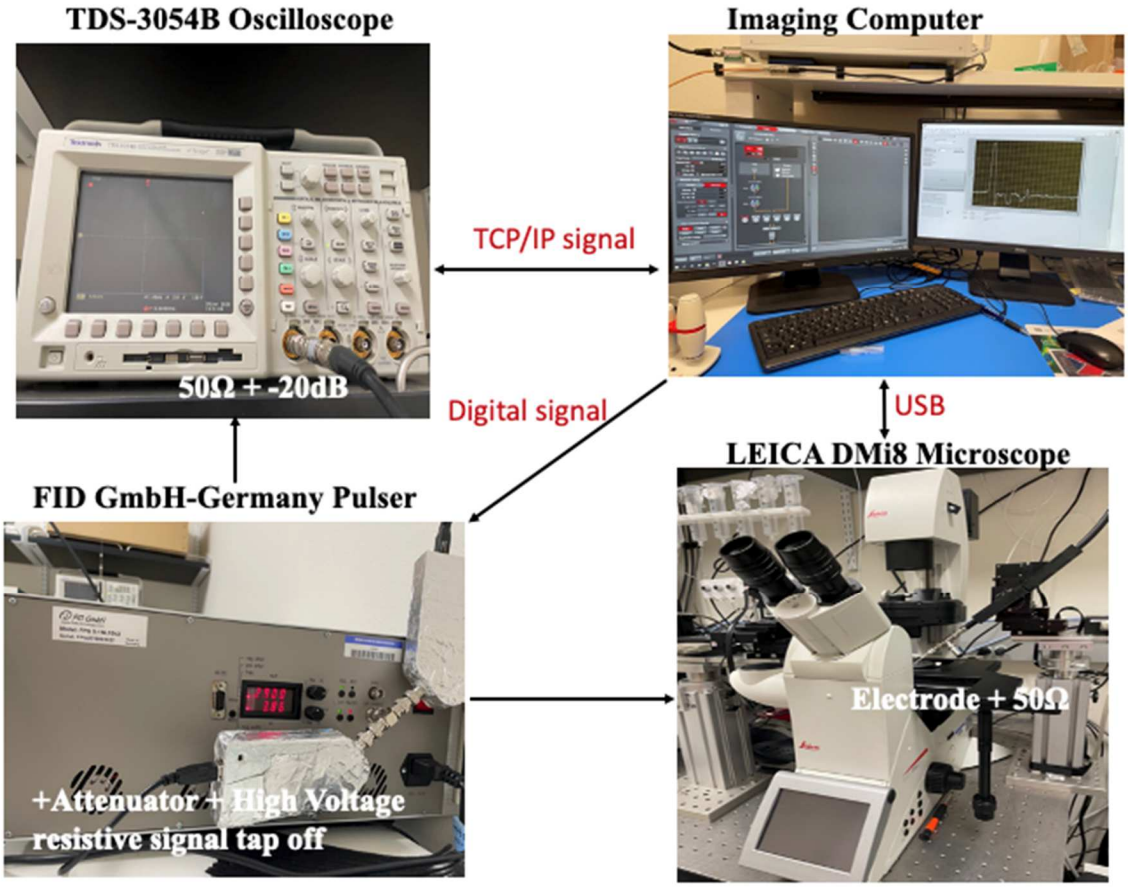


**Figure 2.3 Signal flowchart of the NEP exposure system.** Two-way communication is established between the imaging computer (showing LASX program and Lab VIEW to deliver the pulse and communicate with the oscilloscope) and the oscilloscope. The oscilloscope has 50Ω and -20dB connected to the high voltage cable, There is also a two-way communication between the computer and illumination system and microscope. This allowed precise timing for pulse delivery, which we set as 15 seconds after the recording started.

## 2.5 Threshold E-field amplitudes used for the various pulse durations

To achieve very short pulse durations at low voltages, we have utilized various attenuators that were added either alone or in combination. This is because the NEP

generators tend to generate wider duration pulses than the set pulse duration at a low-voltage operation. This was corrected by increasing the voltage set on the front panel and decreasing the intensity of the pulses using the attenuators. Table 2.1 summarizes the different attenuators used to achieve the desired pulse durations at their respective threshold E-field amplitudes. Of note is that the attenuator allowed to lower the scaled output voltage while maintaining the pulse shape.

**Table 2.1. Summary of the threshold E-field amplitude, the voltage of each pulse duration, and the power of attenuators used**

| Pulse duration (ns) | Threshold E-field amplitude (MV/m) | Threshold Voltage (V) | Attenuation (dB) |
|---|---|---|---|
| 3 | 13.4 | 2700 | -3 |
| 5 | 9.4 | 1900 | -3 |
| 11 | 5.8 | 1180 | -3 |
| 12 | 5.9 | 1200 | -14 |
| 50 | 1.3 | 275 | -22 |

## 2.6 Pulse traces obtained from the short- and long-duration pulse generators

We used two different pulse generators throughout the experiments, FPG 5-1NL10V2 and FPG 5-01NL100V2 (FID GmbH, Germany), to achieve a NEP range of 3 to 50 ns to apply to the cells. The shorter-duration pulser delivers pulses 3 to 11 ns in duration, while the longer-duration pulser delivers pulses 12 to 100 ns in duration. Figures 2.4A and 2.4B show the 3 and 5 ns pulse traces obtained from the shorter-duration pulse generator. The 11 ns pulse duration obtained from the shorter-duration pulser is shown in

Figure 2.4C, and has a trapezoidal shape with a FWHM of 11.4 and a rise time of 4.2 ns, while the 12 ns pulse duration obtained from the longer-duration pulse generator (Figure 2.4D) has a bell-shaped curve with a FWHM of 12.4 ns and a rise time of 5.1 ns. The 50 ns pulse has a trapezoidal shape (Figure 2.4E) with a FWHM of 49.4 ns and a rise time of 6.5 ns.

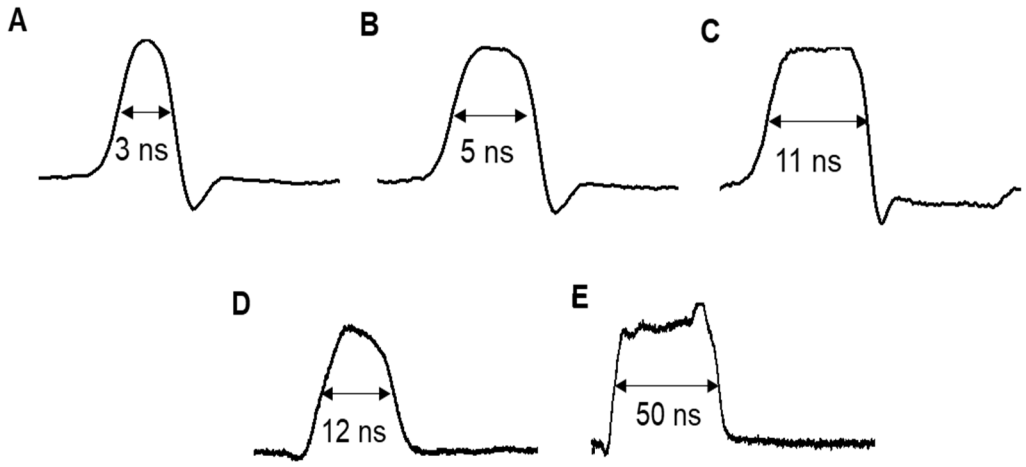


**Figure 2.4 Averaged pulse traces captured by an oscilloscope using the shorter- and longer-duration pulse generators** (A), (B), and (C) unipolar pulse traces for 3, 5, and 11 ns pulses were obtained from the shorter-duration pulser, respectively. (D) and (E) unipolar pulse traces for 12 and 50 ns pulses obtained from the longer-duration pulser, respectively. Pulse traces were captured using an oscilloscope. All pulses were captured at threshold E-field amplitude for evoking responses in bovine chromaffin cells.

## 2.7 Statistical analysis

All the experiments were performed at least two times with two different cell preparations. Data from different experiments were combined, and the results were presented as the mean ± standard error of the mean (SEM). An unpaired Student's t-

test was used to determine the statistical significance between two means of different groups. An ANOVA test was performed to assess the variance among the means of different groups. $p$ values $< 0.05$ were considered statistically significant.

# Chapter 3. RESULTS AND DISCUSSIONS

## 3.1 $Ca^{2+}$ responses in adrenal chromaffin cells exposed to 3ns, 5ns, 11ns, and 50ns at threshold E-fields

### 3.1.1 The ratio of transient and longer-lived $Ca^{2+}$ response is different for different NEP durations

As mentioned in the Introduction, our previous studies showed that the application of a 5 and a 150 ns pulse at the threshold E-field evokes a $Ca^{2+}$ response in all the cells tested (Craviso et al. 2009; Zaklit et al. 2017; Bagalkot et al., 2018). The threshold E-field is defined as the minimum E-field amplitude that elicits a $Ca^{2+}$ response in 100% of the cells, and was determined to be 3-4 MV/m for a 5 ns pulse, and 0.31 MV/m for a 150 ns pulse (Zaklit et al. 2017; Bagalkot et al., 2018). With the acquisition of new pulse generators, E-field intensities were determined to be 13.4 MV/m, 9.4 MV/m, 4.7 MV/m, 2.2 MV/m, and 1.1 MV/m for pulse durations of 3, 5, 11, 25, and 50 ns, respectively (Mansurov, 2021). In this thesis, all experiments employed pulse durations applied at their respective threshold E-Field amplitude.

As shown in Mansurov 2021, the experimental results show two different patterns of $Ca^{2+}$ responses that were dependent on pulse duration. The first is defined as transient

responses where the immediate rise in $Ca^{2+}$ recovers to baseline with $Ca^{2+}$ half-widths shorter than 30 s. The second type of responses is longer-lived responses defined by half-width longer than 30 s or never recover to baseline during 75 s post pulse application. These responses are not desired as the continuous influx of $Ca^{2+}$ can cause damage to the cell. Fig 3.1 shows the transient responses (Figures 3.1A and 3.1C) and longer-lived responses (Figures 3.1B and 3.1D) for 3 and 5 ns. Specifically, 88% ($n$ = 43) and 74% ($n$ = 31) of the cells exhibit transient responses for 3 and 5 ns unipolar pulses, respectively.

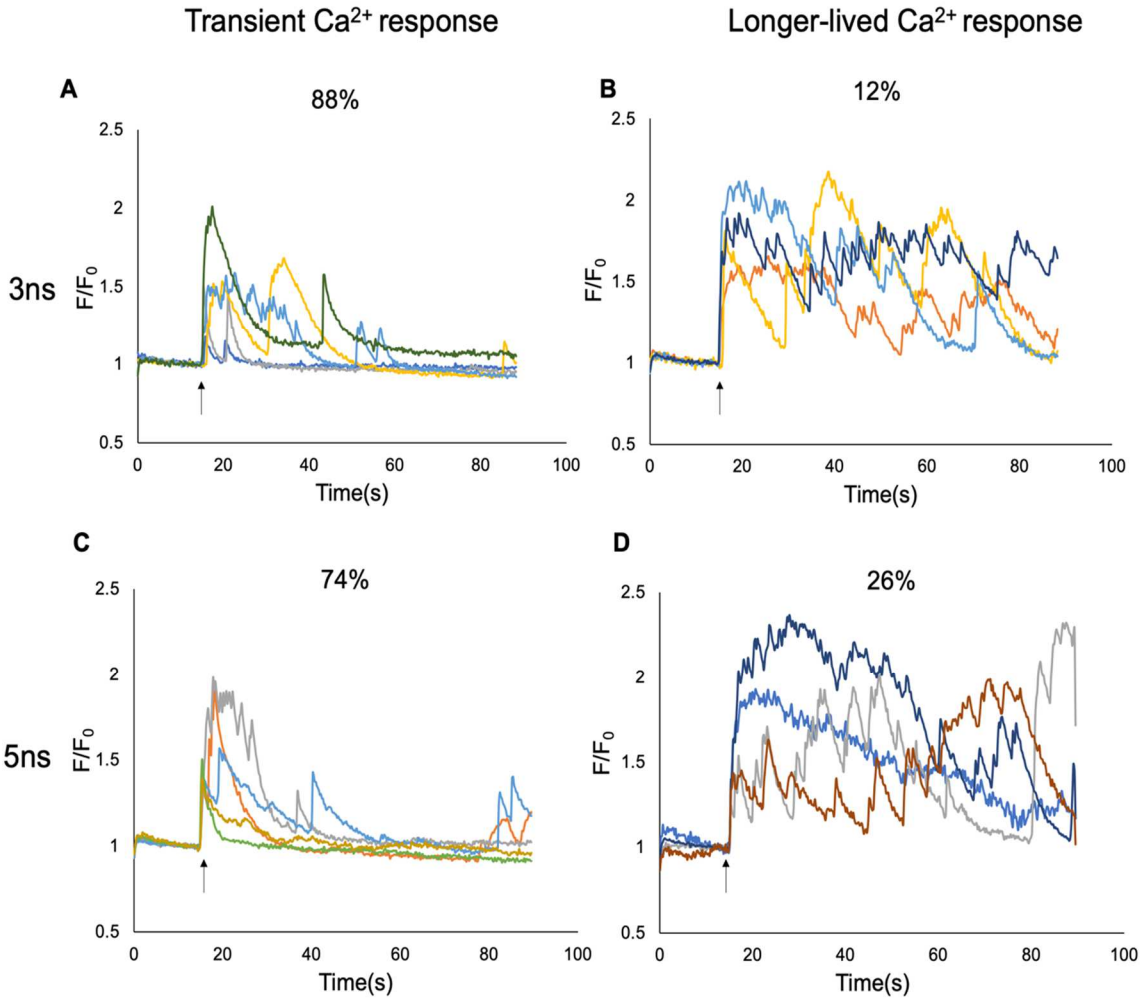


**Figure 3.1 Comparison of $Ca^{2+}$ responses of bovine chromaffin cells exposed to a 3 or 5 ns pulse.** (A) and (C) show representative transient $Ca^{2+}$ responses in cells exposed to a

3 or 5 ns unipolar pulse, respectively. (B) and (D) show representative longer-lived $Ca^{2+}$ responses in cells exposed to a 3 or 5 ns unipolar pulse, respectively. For all pulse durations, pulses were applied at threshold E-field amplitudes. Arrows indicate the time when the pulse was applied.

When the pulse duration was increased to 11 ns (Figure 3.2), the percentage of the cells exhibiting transient versus longer-lived $Ca^{2+}$ responses was significantly reduced to 23% ($n$ = 11) compared to 3 and 5 ns pulses (88 and 74%), and a greater number of cells started to exhibit sustained responses ($n$ = 36) as shown in Figure 3.2B. When the pulse duration was increased to 50 ns, all the cells exhibited longer-lived $Ca^{2+}$ responses ($n$ = 29). Thus, $Ca^{2+}$ responses trended toward a more sustained, higher amplitude $Ca^{2+}$ activity profile as pulse duration increased from 11 ns to 50 ns, with each pulse delivered at its respective E-field threshold. These results show that chromaffin cells can be sensitive enough to show different types of $Ca^{2+}$ responses when exposed to the NEP for the duration of 3, 5, 11, and 50 ns.

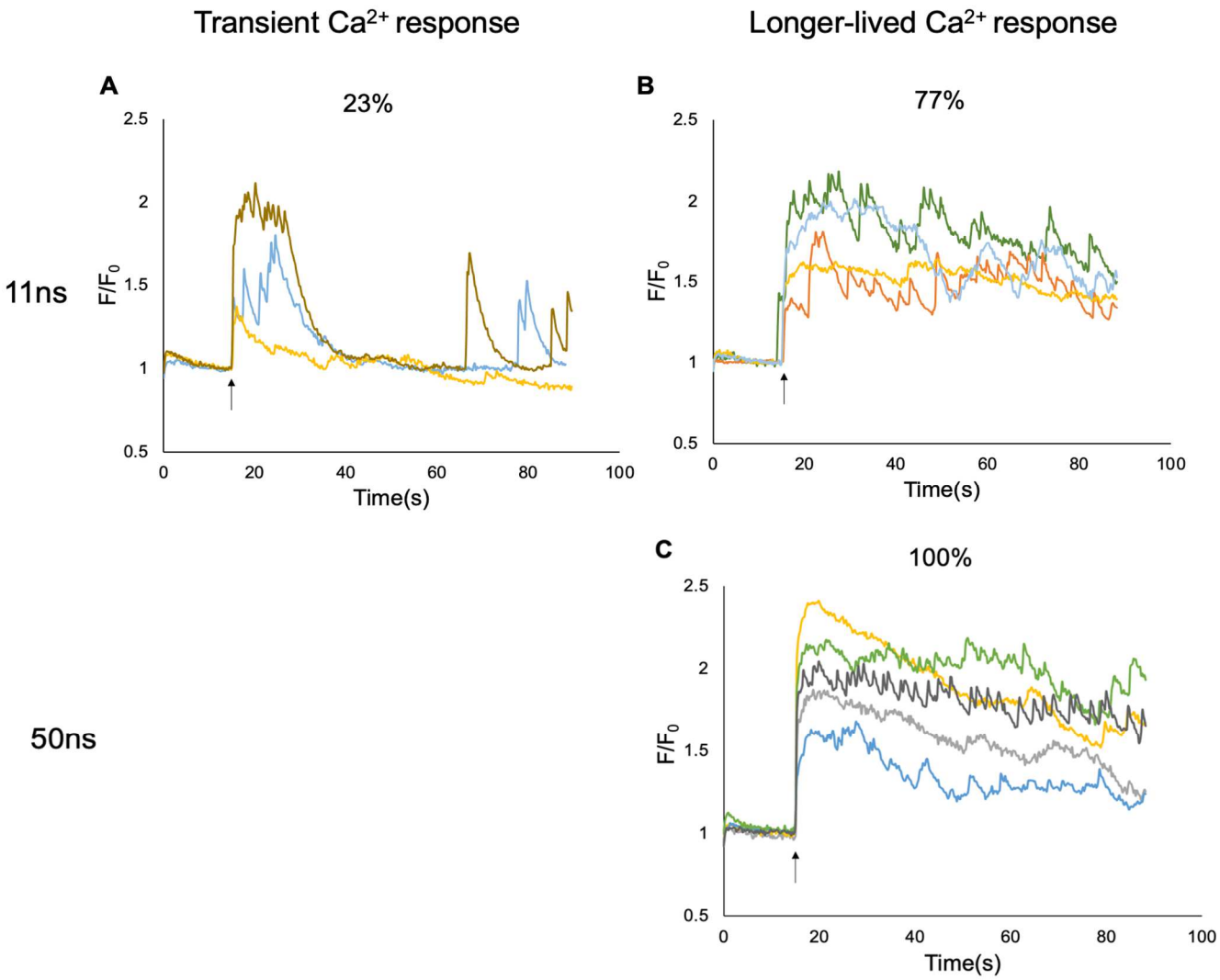


**Figure 3.2 Comparison of $Ca^{2+}$ responses of bovine chromaffin cells exposed to an 11 or 50 ns pulse.** (A) show representative transient $Ca^{2+}$ responses in cells exposed to an 11 ns unipolar pulse. (B) and (C) show representative longer-lived $Ca^{2+}$ responses in cells exposed to an 11 or 50 ns unipolar pulse, respectively. For all pulse durations, pulses were applied at threshold E-field amplitudes. Arrows indicate the time when the pulse was applied**.**

The mean $Ca^{2+}$ response traces for the different pulse durations are plotted together in Figure 3.3 and Figure 3.4  Figure 3.3A, C, and Figure 3.4A show plots averaged separately according to the response type. The orange line shows the averaged transient response at the respective pulse duration and the blue line shows the averaged longer-lived response at the respective pulse duration. For the 50ns duration pulse, since all the cells showed a longer-lived response, a separate plot is not shown. Overall, the percent of cells exhibiting transient versus longer-lived $Ca^{2+}$ responses started to reduce significantly from 11 ns pulse compared to the 3 and 5 ns pulses. Figure 3.3B and D, Figure 3.4B and C show the average plot for all the cells that responded to each duration of pulses. To quantify the peak of the $Ca^{2+}$ amplitude, the peak amplitudes were averaged to obtain the mean $Ca^{2+}$ response magnitudes. The results showed that the 3 ns pulse duration exhibited $1.49 \pm 0.03$ ($n = 49$), and the 5 ns pulse produced $1.64 \pm 0.04$ ($n = 42$), showing that the two pulses resulted in slightly higher mean $Ca^{2+}$ peak amplitude. When the 11 ns pulse was delivered, the cells exhibited $1.73 \pm 0.05$ ($n = 47$), and the 50 ns pulse produced a greater $Ca^{2+}$ response with the mean peak amplitude $2.01 \pm 0.05$ ($n = 30$) ($p < 0.05$).

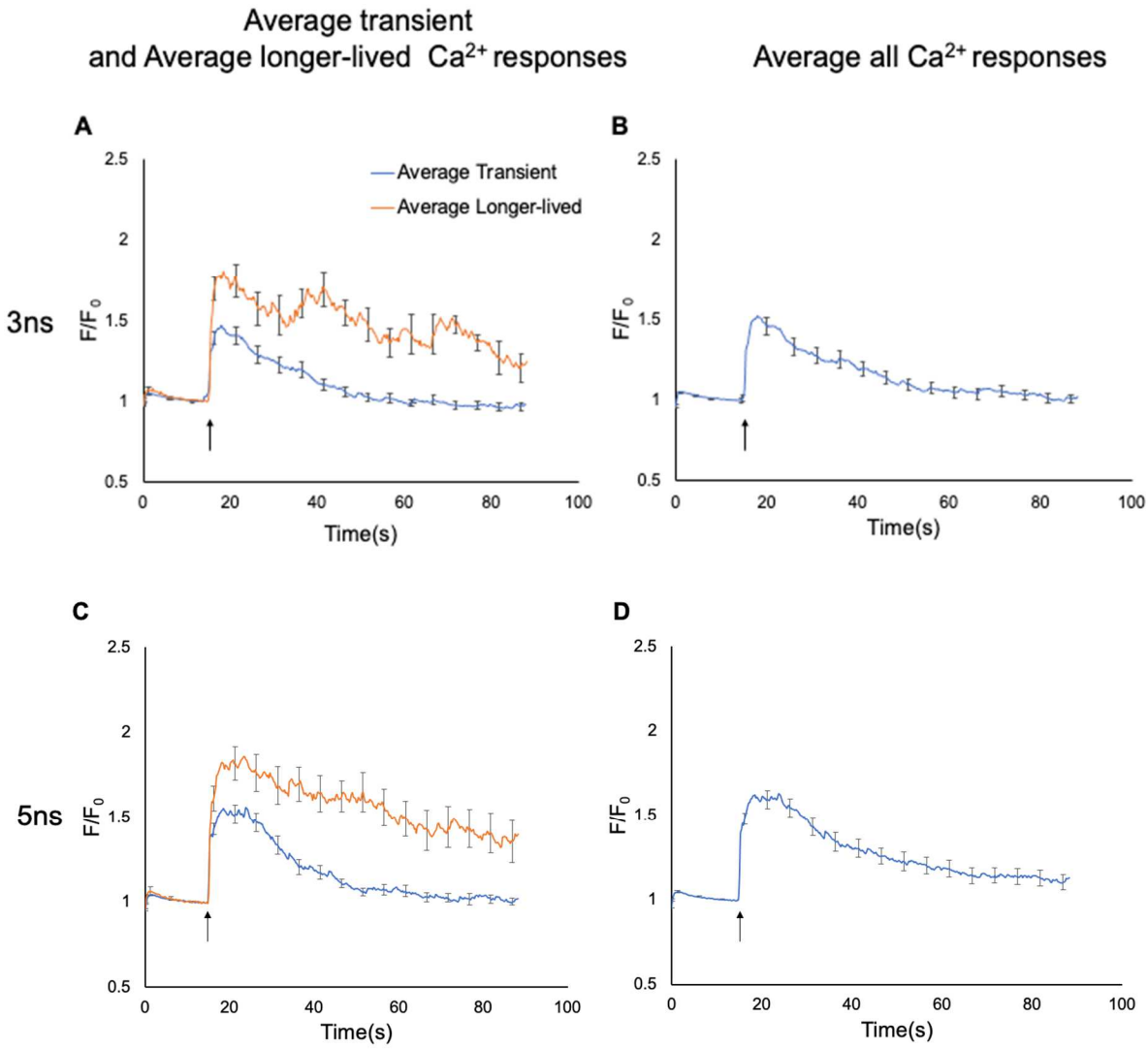


**Figure 3.3 Average transient and longer-lived $Ca^{2+}$ traces for 3 and 5ns pulse.** (A) and (C) show $Ca^{2+}$ response traces that are separated into transient and longer-lived according to the response pattern and are plotted as averaged ± SEM $Ca^{2+}$ responses of cells exposed to the 3 and 5 ns pulses, respectively. (B) and (D) show the average ± SEM $Ca^{2+}$ responses for all the cells exposed to a 3 ($n$ = 49) and 5 ($n$ = 42) ns pulse, respectively. Arrows indicate the time when the pulse was applied.

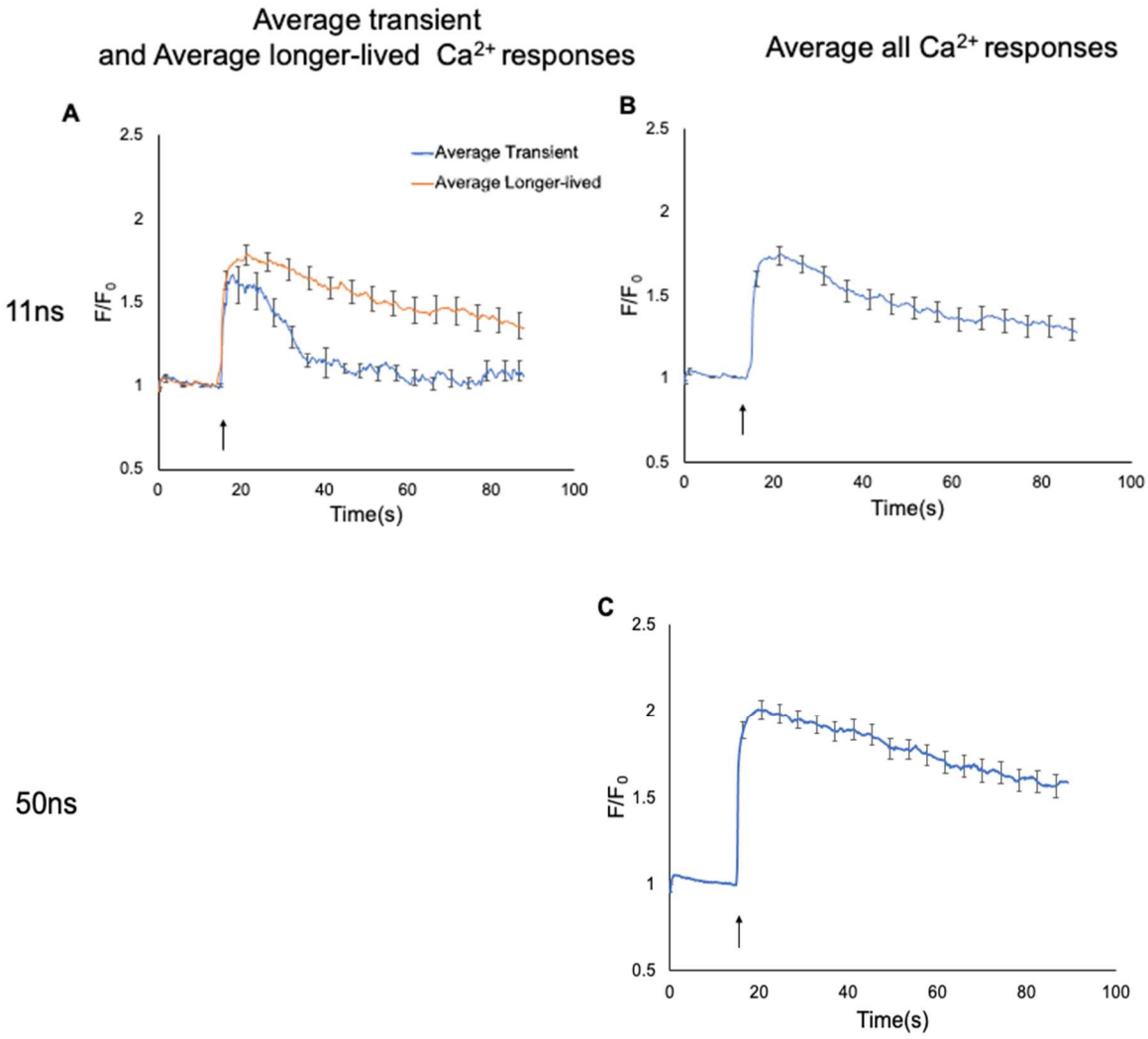


**Figure 3.4 Average transient and longer-lived $Ca^{2+}$ traces for 11 and 50 ns pulse.** (A) shows $Ca^{2+}$ response traces that are separated into transient or longer-lived according to the response pattern and are plotted as averaged ± SEM $Ca^{2+}$ responses of cells exposed to a pulse 11 ns in duration. (B) and (C) show the average ± SEM $Ca^{2+}$ responses for all the cells exposed to a 11 ($n$ = 47) and 50 ns ($n$ = 30) pulse, respectively. Arrows indicate the time when the pulse was applied.

This overall trend of an increasing $Ca^{2+}$ peak amplitude and reduction of recovery to the baseline when pulse duration was increased from 3 to 50ns is visualized in one plot in Figure 3.4. Table 3.1 summarizes these results with average peak amplitude ± SEM. These results are in agreement with our previous studies, meaning that the cells seemed to elicit greater amplitude and much longer-lived $Ca^{2+}$ responses despite the much lower E-field amplitude applied (0.31 MV/m for a 150 ns pulse compared to 3-4 MV/m for a 5 ns pulse), indicating that pulse amplitude appears to affect the response of the cells more than the pulse duration.

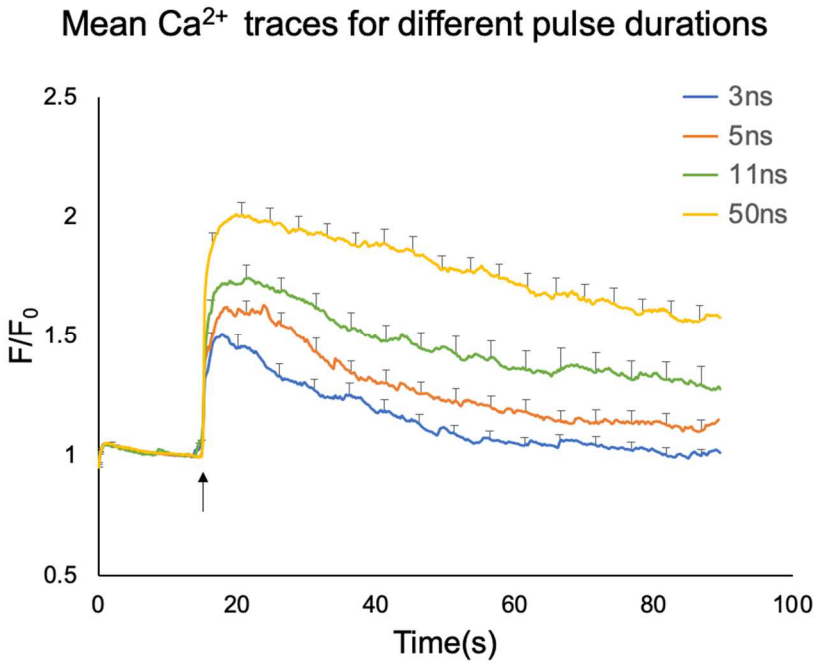


**Figure 3.5 Comparison of the mean $Ca^{2+}$ traces for the different pulse durations.** Traces are plotted as averaged + SEM $Ca^{2+}$ responses of cells exposed to pulses ranging from 3 to 50 ns in duration. Arrow indicates the time when the pulse was applied.

**Table 3.1: Summary of the $Ca^{2+}$ responses of cells exposed to unipolar pulses ranging from 3 to 50 ns in duration, applied at their respective E-field threshold.**

| Unipolar pulse duration | Mean $Ca^{2+}$ peak ± SEM | Mean $Ca^{2+}$ half-width (s) | Cells with half-width < 30 s | Cells with half-width > 30 s | *n* of cells | *p*-value |
|---|---|---|---|---|---|---|
| 3 ns | 1.49 ± 0.03 | 17 | 43 (88%) | 6 (12%) | 49 | - |
| 5 ns | 1.64 ± 0.04 | 22.5 | 31 (74%) | 11 (26%) | 42 | < 0.05 |
| 11 ns | 1.73 ± 0.05 | 43.5 | 11 (23%) | 36 (77%) | 47 | < 0.05 |
| 50 ns | 2.01 ± 0.05 | > 47 | 0 (0%) | 30 (100%) | 30 | < 0.05 |

### 3.1.2 An 11ns pulse from the shorter-duration pulse generator and a 12ns pulse from a longer-duration pulse generator have different shapes, but the $Ca^{2+}$ responses of the cells are similar

As mentioned, two different pulse generators were used for the experiments, the FPG 5-1NL10V2 and the FPG 5-01NL100V2 (FID GmbH, Germany) achieved a range of NEPs from 3 to 11 ns in duration, and 12 to 100 ns in duration, respectively. One noticeable difference is the shape of the 11 ns (Figure 3.5A) and 12ns (Figure 3.5B) pulses. Thus, we compared the $Ca^{2+}$ response of the cells evoked by a 12 ns pulse applied using the longer-duration pulse generator to the $Ca^{2+}$ response of the cells when an 11 ns pulse was applied using the shorter-duration pulse generator. We also identified the threshold E-field amplitude of the 12 ns pulse and compared it to that of the 11 ns pulse.

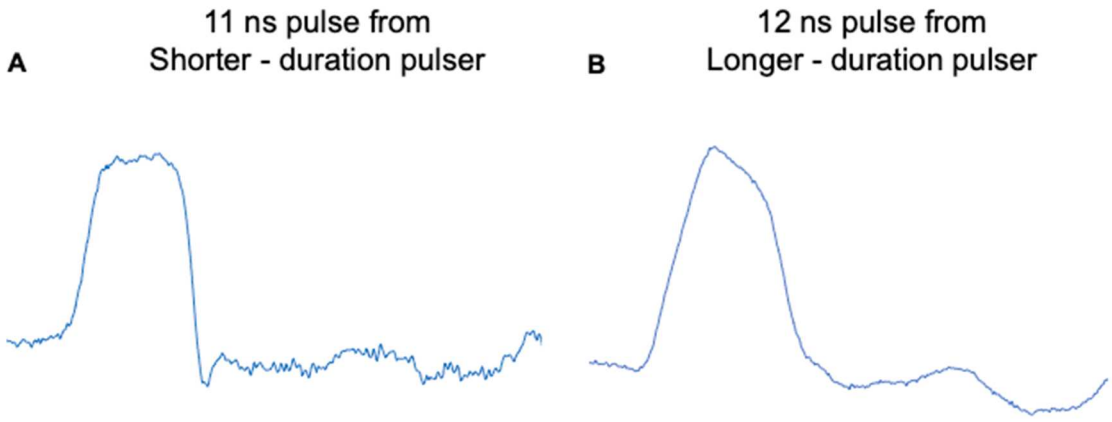


**Figure 3.6 11ns and 12ns pulse traces from two different pulse generators.** (A) shows a 11ns pulse trace generated from the shorter-duration pulser. (B) shows a 11ns pulse trace generated from longer-duration pulser. Pulse traces were captured using an oscilloscope.

The representative $Ca^{2+}$ traces of longer-lived and shorter-lived responses are shown in Figure 3.6A and Figure 3.6B when a 11ns pulse was applied to the cells. The representative traces of longer-lived and shorter-lived responses shown in Figure 3.6C and Figure 3.6D are when a 12 ns pulse using a longer-duration pulse generator was applied to the cells. Among the cells exposed to 11 and 12 ns pulse, 23% showed a transient $Ca^{2+}$ response when a 11 ns pulse was used while 25% of the cells showed a transient response when a 12 ns pulse was used. For the longer-lived $Ca^{2+}$ activity, 77% of the cells exhibited longer-lived activity with 11 ns pulses, and 75% of the cells exhibited longer-lived activity for the 12 ns pulses. This result indicates that the cells exhibited the same transient and longer-lived response ratio despite the difference in the shape of the pulses.

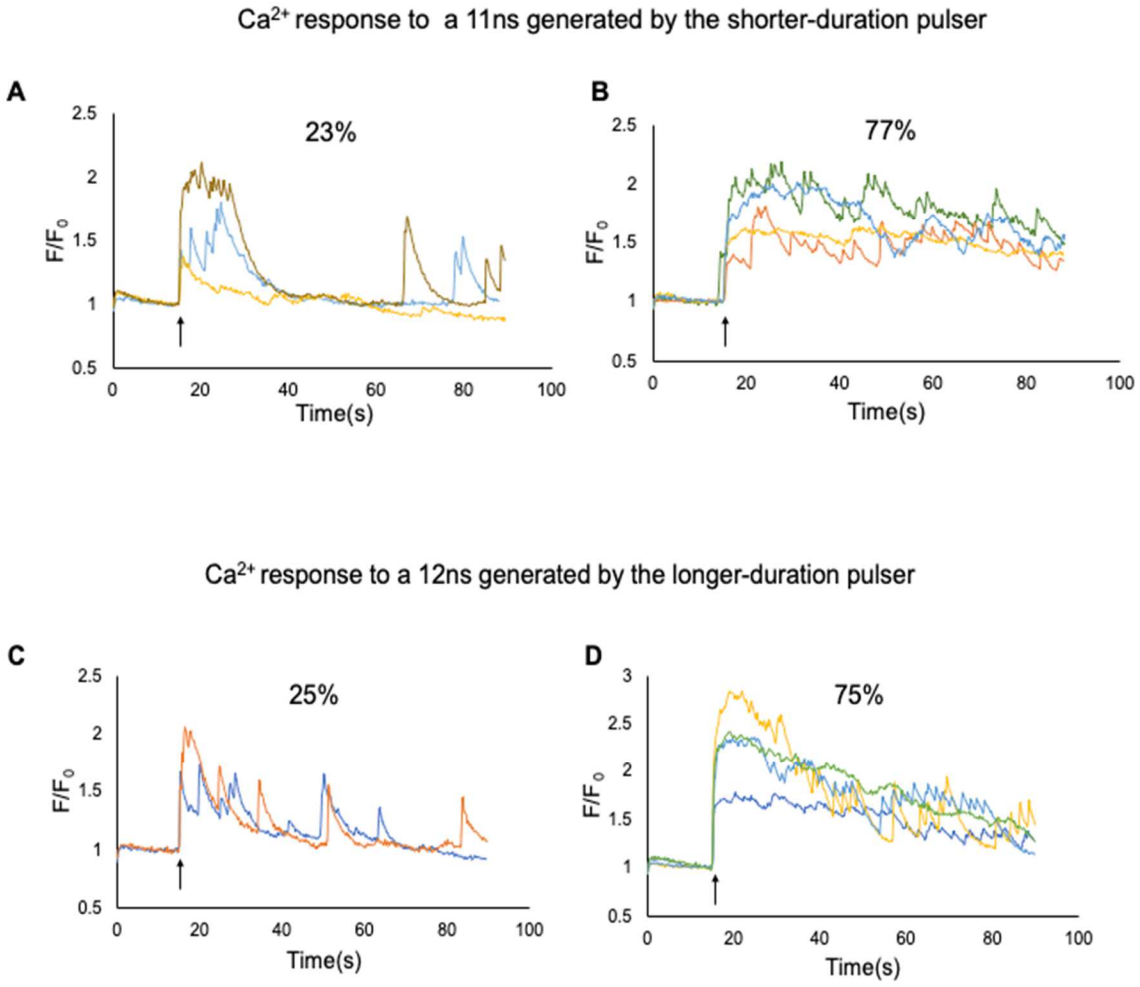


**Figure 3.7 Transient and longer-lived $Ca^{2+}$ responses of the cells exposed to 11 ns and 12 ns pulse from the two different pulsers.** The percentage of the short and long-duration responses are shown on the top of each plot showing the representative $Ca^{2+}$ responses. (A) and (B) are representative $Ca^{2+}$ responses of the cells exposed to 11ns pulse generated by shorter-duration pulser. (C) and (D) are representative $Ca^{2+}$ responses of the cells exposed to 12ns pulse generated by longer-duration pulser.

Figures 3.7A and B show the average plot for all the cells that responded to each pulse from the shorter- and longer-duration pulser, respectively. To quantify the peak of the $Ca^{2+}$ amplitude, the peak amplitudes were averaged to obtain the mean $Ca^{2+}$ magnitudes. The results showed that the 11ns unipolar pulse from shorter-duration pulser exhibited a peak amplitude of 1.71 ± 0.05 ($n$ = 47), and the 12 ns unipolar pulse from longer-duration pulser produced a peak amplitude of 2.11 ± 0.40 ($n$ = 8).

Although we will need more numbers of cells from the longer-duration pulser, the results show that the percentage of transient and longer-lived $Ca^{2+}$ responses remain similar between the two pulses from different pulser when the pulse duration is similar. Meanwhile, the amplitude of the $Ca^{2+}$ response seems to be affected. Since the result for the 12 ns pulse with the longer-duration pulser is from only one experiment ($n$ = 8), it is hard to conclude if this difference is significant. Of note is that the area under the curve of each applied pulse came out to be 13.6 for the 11 ns pulse generated by the shorter-duration pulser and 14.1 for the 12 ns pulse generated by the longer-duration pulser. This number represents the electrical charge each pulse generator produces. The higher amplitude of $Ca^{2+}$ response when a 12 ns pulse is applied (Figure 3.8) can be the result of the difference in the number of electrons, which is an electrical charge accumulated in the cell membrane.

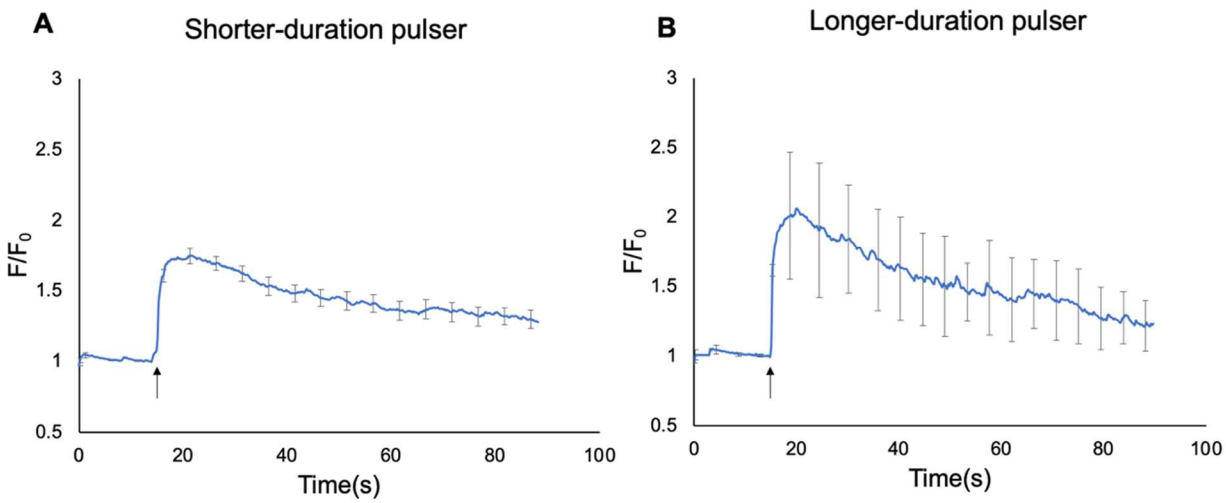


**Figure 3.8 Mean $Ca^{2+}$ responses of cells obtained from a pulse delivered from a longer-duration and shorter-duration pulser.** (A) Trace is plotted as averaged ± SEM $Ca^{2+}$ responses of cells ($n$ = 47) exposed to 11 ns unipolar pulse generated from shorter-duration pulser. (B) Trace is plotted as averaged ± SD $Ca^{2+}$ responses of cells ($n$ = 8) exposed to 12 ns unipolar pulse generated from longer-duration pulser.

For all the following experiments employing 11 ns pulses, the shorter-duration pulse generator was used.

## 3.2 The source of the $Ca^{2+}$ response was extracellular for 11 and 50 ns pulses

Our group has previously found that a single 5 ns pulse applied at threshold E-field amplitude does not cause $Ca^{2+}$ release from intracellular stores (Craviso et al. 2008; Zaklit et al. 2017). To determine whether the source of $Ca^{2+}$ responsible for the NEP-evoked increases in $Ca^{2+}$ was intracellular or extracellular and whether a release of $Ca^{2+}$ from internal stores contributed to the longer-lived $Ca^{2+}$ transients, cells were imaged in $Ca^{2+}$-free BSS with 1 mM EGTA in the solution and exposed to pulses 11 and 50 ns in duration. These pulse durations were tested for the following reasons: An 11 ns pulse represents the

duration at which the $Ca^{2+}$ responses start to exhibit a larger percentage of longer-lived activity compared to transient activity, and 50 ns is the maximum pulse duration tested because this is the duration at which all the cells exhibit a longer-lived activity.

Figure 3.9 shows the representative $Ca^{2+}$ responses when a 11 ns and 50 ns unipolar pulse was applied in $Ca^{2+}$-free BSS with 1 mM EGTA. As shown in Figure 3.9A and Figure 3.9C, the removal of external $Ca^{2+}$ completely abolished the response of all the cells to NEP exposure for both 11 and 50 ns pulse durations, indicating that there was no $Ca^{2+}$ release from intracellular stores and the $Ca^{2+}$ responses observed were due to $Ca^{2+}$ entry into cells.

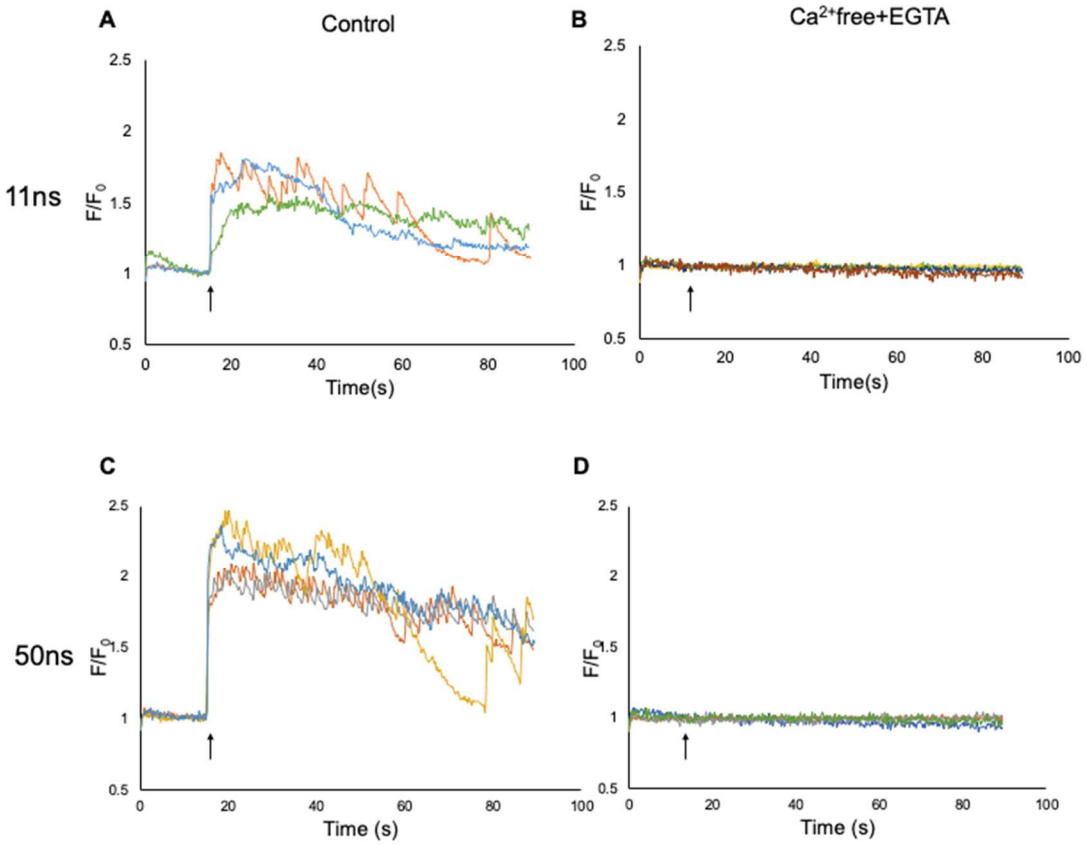


**Figure 3.9 Representative $Ca^{2+}$ responses of the cells to an 11 and a 50 ns pulses with and without extracellular $Ca^{2+}$.** Representative $Ca^{2+}$ responses in cells exposed to a (A), (B) 11 ns pulse ($n$ = 13 for control; 16 for $Ca^{2+}$-free), and (C), (D) 50 ns pulse ($n$ = 13 for control; 16 for $Ca^{2+}$-free). Each pulse was applied in the presence and absence of extracellular $Ca^{2+}$. In the absence of external $Ca^{2+}$, 1 mM EGTA was added. Arrows indicate the time when the pulse was applied.

Figure 3.10 shows the averaged $Ca^{2+}$ responses when an 11 ns and a 50 ns pulse was applied in $Ca^{2+}$-free BSS with 1 mM EGTA and 2 mM $Ca^{2+}$ BSS (control). The cells did not show any $Ca^{2+}$ response as marked in blue traces in Figures 3.10A and 3.10B when there was no external $Ca^{2+}$ present for both 11 and 50 ns pulse duration. The mean

amplitude of the control condition's $Ca^{2+}$ response peak shown in Figures 3.10A and 3.10(B) matched the mean $Ca^{2+}$ response to the pulse of an11 and a 50 ns pulse.

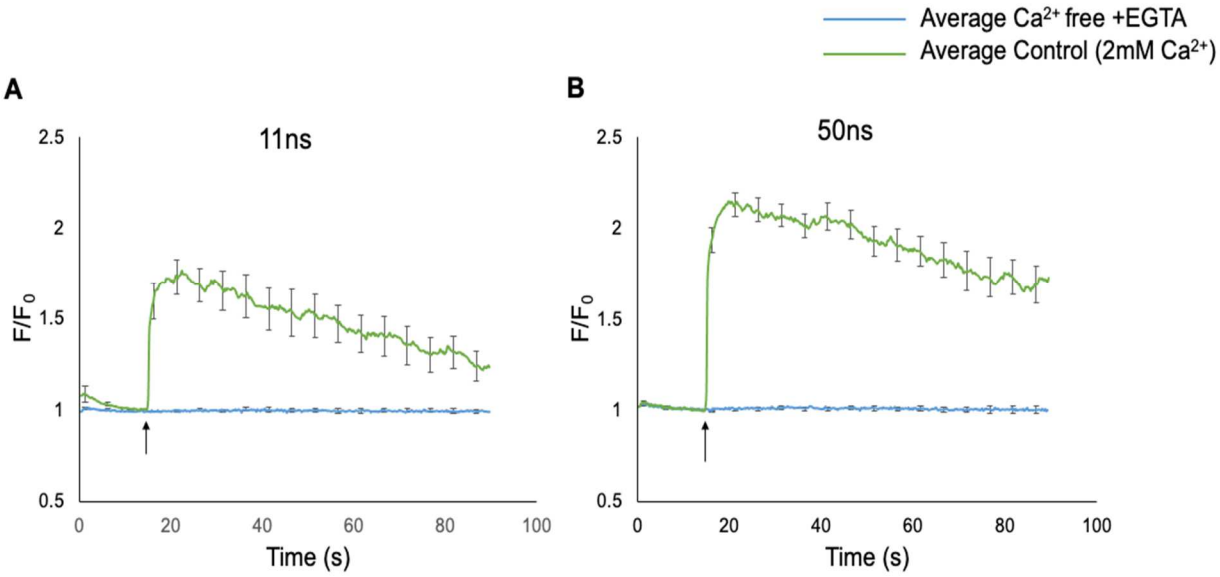


**Figure 3.10 Effect of extracellular $Ca^{2+}$ on the $Ca^{2+}$ response of the cells exposed to 11 and 50 ns unipolar pulses.** Averaged $Ca^{2+}$ responses ± SE in cells exposed to a (A) 11 ns pulse ($n$ = 13 for control; 16 for $Ca^{2+}$-free), and (B) 50 ns pulse ($n$ = 13 for control; 16 for $Ca^{2+}$-free). Each pulse was applied in the presence and absence of extracellular $Ca^{2+}$. The blue line indicates the control conditions with external 2mM $Ca^{2+}$ present, and the green line indicates the $Ca^{2+}$-free condition with 1mM EGTA added. Arrows indicate the time when the pulse was applied.

### 3.2.1 VGCCs account for the majority of $Ca^{2+}$ influx when the pulse duration is shorter than 11 ns

Craviso et al. 2010 reported that in isolated adrenal chromaffin cells, a single 5 ns pulse triggers a rise in $[Ca^{2+}]_i$ that involves $Ca^{2+}$ influx solely via voltage-gated calcium channels (VGCCs). Another recent study from our group has shown that in isolated adrenal

chromaffin cells, a single 2 ns pulse triggers a rise in $[Ca^{2+}]_i$ that involves $Ca^{2+}$ influx solely via voltage-gated calcium channels (VGCCs) (Zaklit et al., 2021). However, Bagalkot et al. 2019 reported that, with longer duration pulse (150 ns), delivered at just above the threshold E-field, elicited $Ca^{2+}$ influx not only via VGCCs but also via the non-VGCCs involved pathway. When 150 ns unipolar pulse was applied, around 60-70% of $Ca^{2+}$ influx was calculated to be through VGCC and 30-40% of $Ca^{2+}$ influx is through non-VGCC.

With these studies in mind and after determining that the source of $Ca^{2+}$ was extracellular, we next wanted to investigate what aspect of the $Ca^{2+}$ entry pathway into cells is responsible for the basis of the changes in the characteristics of NEP-evoked $Ca^{2+}$ responses as pulse duration increases. Thus, to determine the pulse duration range at which $Ca^{2+}$ entry would involve only VGCCs, cells were exposed to a 3, 5, 11 or 50 ns pulse under treatment with a cocktail of organic VGCC blockers selective for each $Ca^{2+}$ channel type. The cocktail of blockers contained 100 nM ω-agatoxin IVA, 20 nM ω-conotoxin GVIA, and 20 μM nitrendipine to block P/Q-, N-, and L-type $Ca^{2+}$ channels, respectively. All these channels are known to be expressed in bovine chromaffin cells (García et al., 2006). Each blocker was used at a concentration previously used by our group to block VGCCs in bovine chromaffin cells (Craviso et al., 2010; Bagalkot et al., 2018).

Figure 3.11 and Figure 3.12 show the representative $Ca^{2+}$ responses of the cells evoked by a 3, 5, 11 or 50 ns pulse in the presence or absence of the cocktail of VGCC blockers. The results show that blocking VGCCs caused complete inhibition of $Ca^{2+}$ influx triggered by a 3 ns and almost complete inhibition with very little response to a 5 ns pulse, as Figure 3.11A and B show. This result is consistent with our previous observations

(Craviso et al. 2010). Interestingly, we found that increasing the pulse duration from 5 to only 11 ns resulted in the inability of a cocktail of VGCC inhibitors to fully block the response, as Figure 3.12C shows. When the pulse duration further increased to 50 ns, only a small blockade of the $Ca^{2+}$ response by the cocktail of VGCC inhibitors was observed. In addition, cells that do not show $Ca^{2+}$ influx response were greatly reduced when the pulse duration was 11 ns and 50 ns, as seen in the number of the cells that responded in Figure 3.12B and D. These results indicate that pulses less than 11 ns in duration cause $Ca^{2+}$ influx primarily through VGCCs.

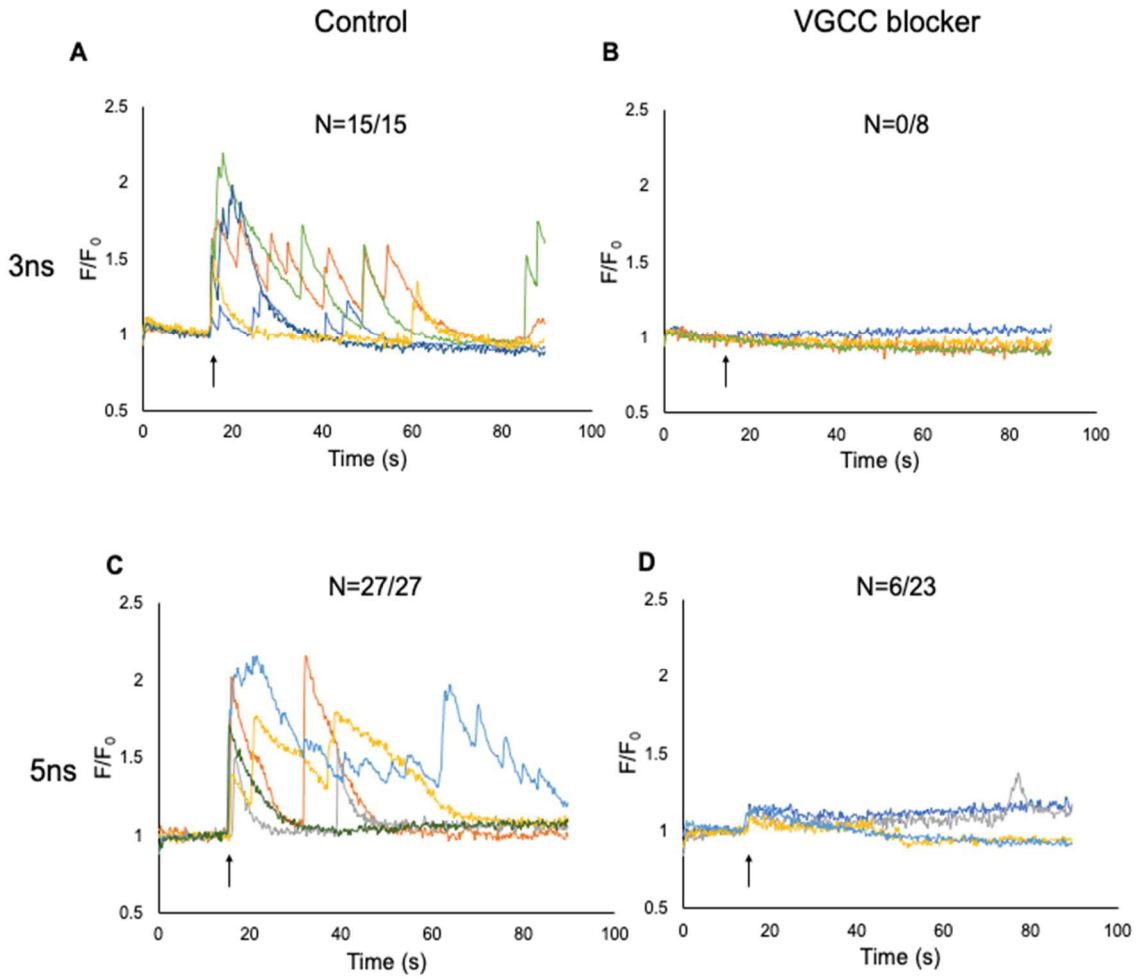


**Figure 3.11 Representative plots showing the effect of pulse duration on the $Ca^{2+}$ responses in cells exposed to a 3 and a 5ns pulse in the absence and presence of VGCC blockers.** Results shown are representative cell responses for cells exposed to a (A) and (B), to a 3 ns pulse, and (C) and (D) to a 5 ns pulse in the absence and presence of a cocktail of VGCC channel inhibitors containing 100 nM ω-Agatoxin IVA, 20 nM ω-Conotoxin GVIA and 20 μM nitrendipine. Cells were incubated for 60 min at 37 °C with the blockers before imaging. The number of the cells that responded out of all cells that have been tested is shown on top of each plot. Arrows indicate the time when the pulse was applied.

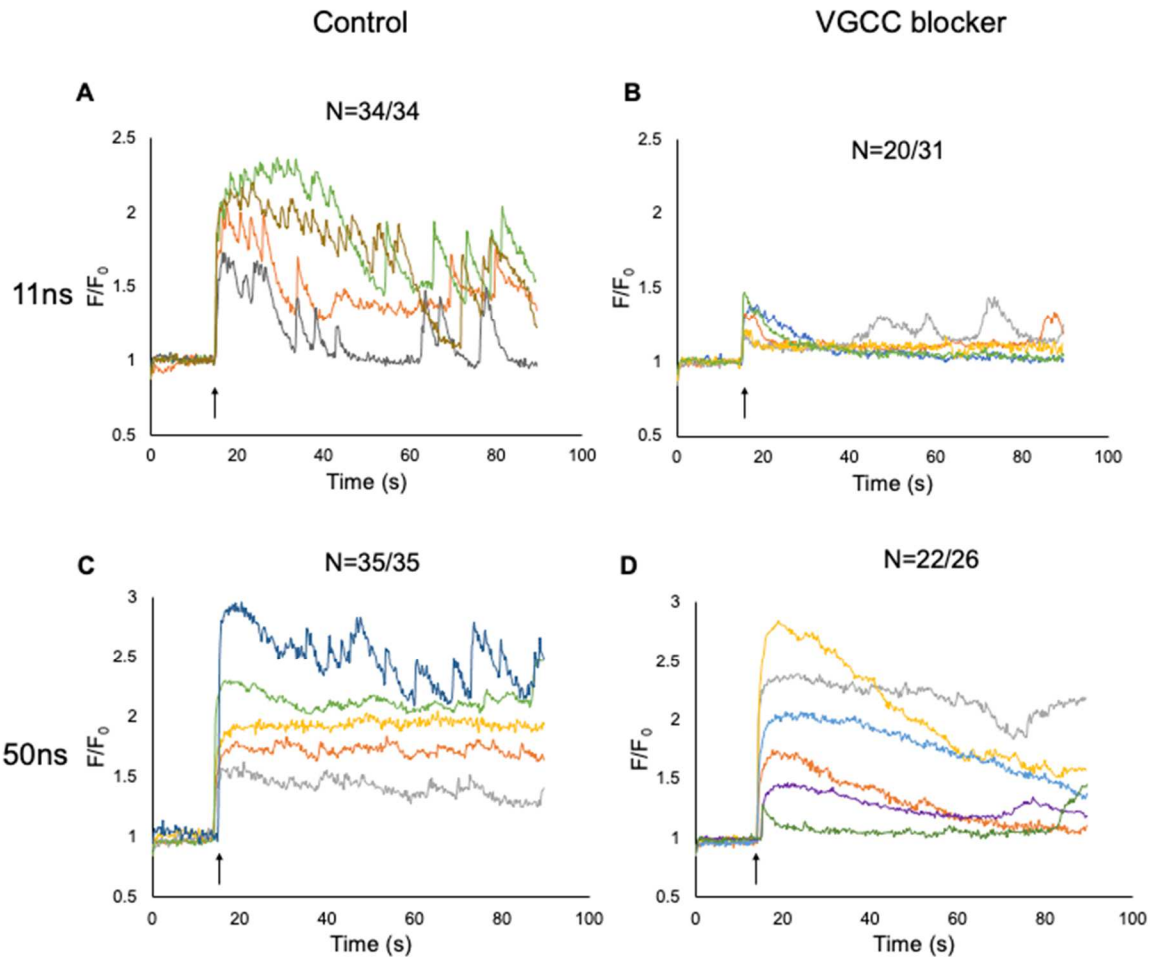


**Figure 3.12 Representative plots showing the effect of pulse duration on the $Ca^{2+}$ responses in cells exposed to an 11 and a 50 ns pulse in the absence and presence of VGCC blockers.** Results shown are representative cell responses for cells exposed to a (A) and (B) to an 11 ns pulse, and (C) and (D) to a 50 ns pulse in the absence and presence of a cocktail of VGCC channel inhibitors containing 100 nM ω-Agatoxin IVA, 20 nM ω-Conotoxin GVIA and 20 µM nitrendipine. Cells were incubated for 60 min at 37 °C with the blockers before imaging. The number of the cells that responded out of all cells that have been tested is shown on top of each plot. Arrows indicate the time when the pulse was applied.

The averaged plots shown in Figure 3.13 demonstrate that blocking VGCCs caused complete inhibition of $Ca^{2+}$ influx triggered by a 3 and 5 ns pulse. This result is consistent with our previous observations (Craviso et al., 2010). The mean peak amplitude for each

condition are 1.45 ± 0.07 ($n$ = 8) for the control and 1.04 ± 0.03 ($n$ = 15) for VGCCs cocktail treated cells exposed to a 3 ns pulse, 1.68 ± 0.05 ($n$ = 27) for the control and 1.08 ± 0.01 ($n$ = 23) VGCCs cocktail treated cells exposed to a 5 ns pulse, 1.97 ± 0.04 ($n$ = 34) for the control and 1.19 ± 0.02 ($n$ = 31) VGCCs cocktail treated cells exposed to a 11 ns pulse, and 2.14 ± 0.06 ($n$ = 35) for the control and 1.62 ± 0.09 ($n$ = 26) VGCCs cocktail treated cells exposed to a 50 ns pulse .

Here, it is notable that when the pulse duration is increased to 11 ns, blocking VGCCs caused the magnitude of the $[Ca^{2+}]_i$ reduced by 80% ($p < 0.05$). For a 50 ns pulse, the cocktail of blockers reduced the magnitude of the rise in $[Ca^{2+}]_i$ by 50% ($p < 0.05$).

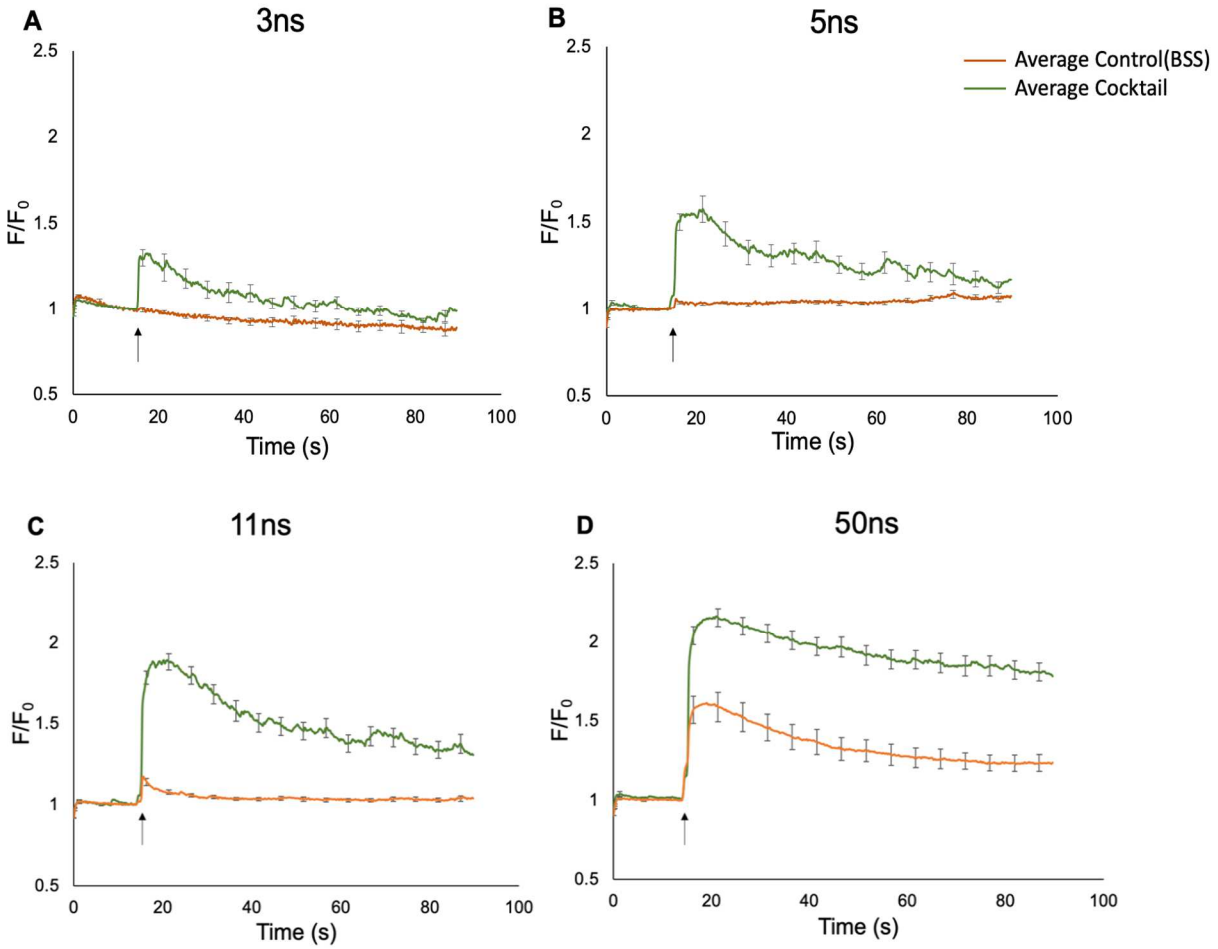


**Figure 3.13 Average plots showing the effect of pulse duration on the $Ca^{2+}$ responses in cells exposed to a 3, 5, 11, and 50 ns pulse in the absence and presence of VGCC blockers.** Results are plotted as the averaged cell responses ± SEM for cells exposed to a (A) 3 ns, (B) 5 ns, (C) 11 ns, and (D) 50 ns pulse in the absence and presence of a cocktail of VGCC channel inhibitors containing 100 nM ω-agatoxin IVA, 20 nM ω-conotoxin GVIA and 20 µM nitrendipine Cells were pretreated with the blockers for 60 min at 37 °C. Arrows indicate the time when the pulse was applied.

In Figure 3.14, the percentage of the cells that responded under each condition is summarized in a bar graph. When cells were treated with the cocktail of VGCC blockers, we found complete elimination of the $Ca^{2+}$ response in all cells exposed to a 3 ns pulse, while the number of cells responding to a 5 ns pulse was significantly reduced compared

to the control, with only 26% ($n$ = 6/23) of the cells responding to the stimulus. When the pulse duration was increased to 11 ns, 65% ($n$ = 20/31) of the cells have shown a response. At the pulse duration of 50 ns, 22 cells out of 26 total, which is 85% of cells responded to the pulse. Figure 3.15 shows the magnitude of the $Ca^{2+}$ responses of those cells that exhibited a response to each pulse. Overall, the magnitude of the increase in fluorescence intensity was also significantly reduced compared to the control. The results indicate that blockers of VGCCs entirely blocked the NEP-induced increases in $[Ca^{2+}]_i$ when a 3 ns pulse was applied, significantly reduced the NEP-induced increases in $[Ca^{2+}]_i$ when a 5 ns pulses were applied, and also largely reduced the NEP-induced increases in $[Ca^{2+}]_i$ when a 11 ns pulses were applied and by 50 ns, the blockers of VGCCs only partially blocked the NEP-induced increase in $[Ca^{2+}]_i$.

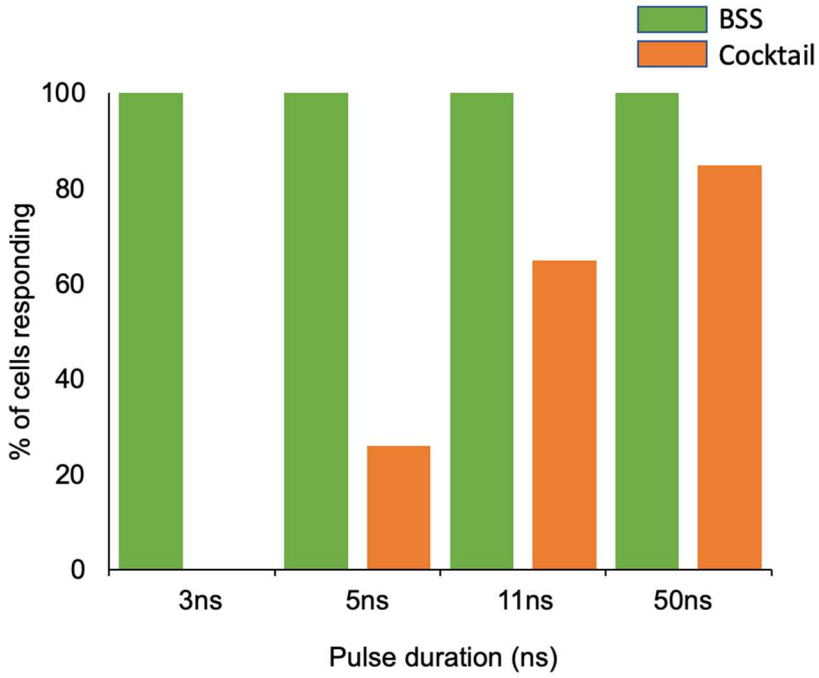


**Figure 3.14 The effect of pulse duration on the number of cells responding to NEPs in the absence and presence of the cocktail of VGCC inhibitors.** The orange bar shows the percentage of cells responding to the pulse in the presence of the cocktail at each pulse duration. The green bar shows the percentage of cells responding to the pulse in the absence of the cocktail at each pulse duration.

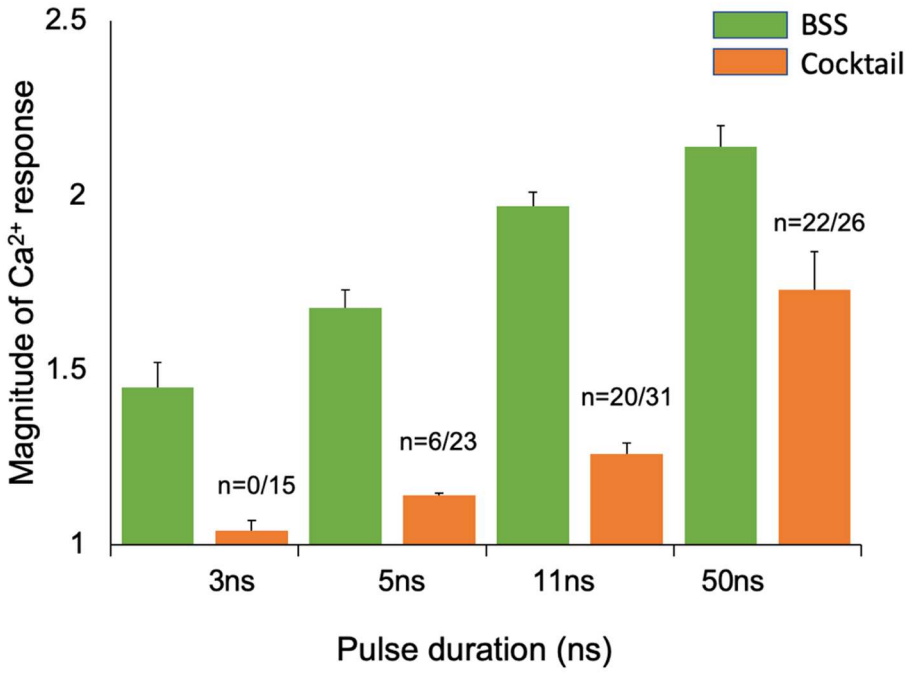


**Figure 3.15 The effect of pulse duration on the number of cells responding and the magnitude of the $Ca^{2+}$ response in cells exposed to NEPs in the absence and presence of the cocktail of VGCC inhibitors.** Shown is the magnitude of the $Ca^{2+}$ response as a function of pulse duration, both in the absence and presence of the cocktail of VGCC blockers. In each case, *n* represents the number of cells responding to the pulse out of the total number of cells tested for each pulse duration.

Taken together, it can be inferred that for pulse durations less than 11 ns, VGCCs account for the majority of $Ca^{2+}$ influx evoked by a pulse, and increasing the pulse duration to 50 ns causes $Ca^{2+}$ influx not only via VGCCs but also through the path independent from VGCCs such as other types of cation channels that are permeable to $Ca^{2+}$.

### 3.2.2 $Ca^{2+}$ influx was not observed for all pulse duration when $Ca^{2+}$channels were blocked with $Cd^{2+}$

$Cd^{2+}$ is an inorganic, nonselective blocker for VGCCs in cells. Our research group has used $Cd^{2+}$ to evaluate the role of these channels in the $Ca^{2+}$ response of the cells to 150 ns pulses (Bagalkot et al., 2018). We found that all pathways of $Ca^{2+}$entry, including VGCC-dependent and non-VGCC-dependent, were inhibited by $Cd^{2+}$. Thus, for the next step, we tested pulses 11 and 50 ns in duration with $Cd^{2+}$ since with this pulse duration, $Ca^{2+}$ responses were still observed in the presence of the cocktail of VGCC blockers. For the experiment, cells were exposed to the pulses in BSS containing 200 μM $CdCl_2$ to compare with the control condition of cells exposed to the same pulse duration in BSS containing 2 mM $CaCl_2$. As shown in Figure 3.16 and consistent with our previous study (Bagalkot et al. 2018), we found that there was no rise in $[Ca^{2+}]_i$ when an 11 or 50 ns pulse was applied with $Cd^{2+}$ present in the BSS. The average cell responses ± SEM for Figure 3.14A, where an 11ns applied is 1.02 ± 0.01 for the $Cd^{2+}$ present condition, while averaged cell responses for the control condition is 1.93 ± 0.27. The average cell responses ± SEM for Figure 3.16B, where 50 ns pulse was applied, is 1.02 ± 0.01 for the $Cd^{2+}$ present condition and 2.07 ± 0.27 for the control condition. These results indicate that $Cd^{2+}$ blocked all $Ca^{2+}$ entry pathways, including VGCCs and undefined non-VGCC pathways.

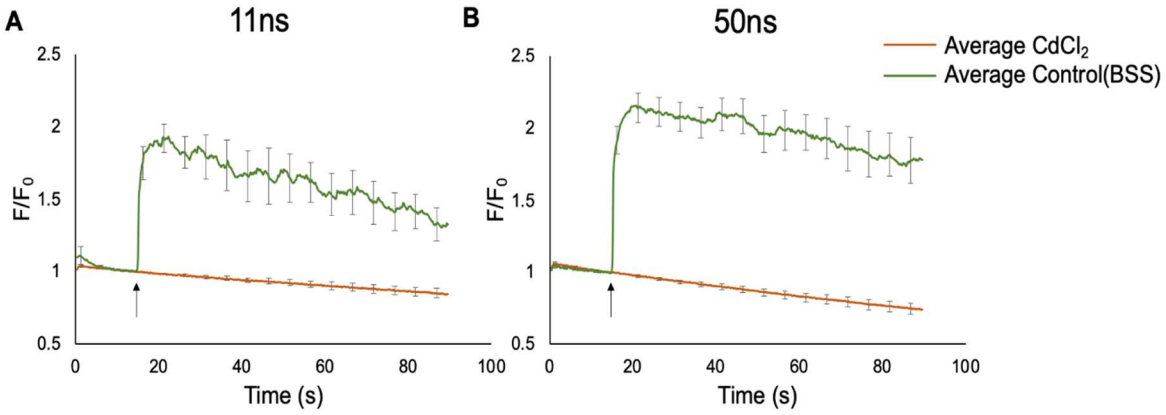


**Figure 3.16 Comparison of $Ca^{2+}$ responses in cells exposed to an 11 and 50 ns pulse in the presence and absence of $Cd^{2+}$.** Averaged cells responses ± SEM for cells exposed to a (A) 11 ns pulse ($n$ = 8 for control; 8 for $Cd^{2+}$) and (B) 50 ns pulse ($n$ = 8 for control; 8 for $Cd^{2+}$). For the experimental condition, cells were pretreated with 200 µM $Cd^{2+}$ for 30 min at 37 °C. Arrows indicate the time when the pulse was applied.

### 3.2.3 YO-PRO-1 uptake was not detected with exposure to any pulse durations

Since the results from the previous sections, when the 50 ns duration pulse was applied to the cells, longer-lived $Ca^{2+}$ influx was the dominant response, we wanted to investigate whether there is a possibility of electro permeabilization that allow YO-PRO-1 uptake into cells. While monitoring the YO-PRO-1 uptake into the cells, 50 ns pulses in duration were applied at threshold E-field to the cells in BSS containing 2 µM YO-PRO-1. As a result, for the cells exposed to a single 50 ns pulse, YO-PRO-1 uptake was not observed (data not shown). In short, even though $Ca^{2+}$ was still entering the cells through the pathway that is non-VGCCs, which is blocked by $Cd^{2+}$, chromaffin cells still did not show YO-PRO-1 uptake. This indicates that $Ca^{2+}$ entered the cells when exposed to a single 50 ns pulse via a pathway that does not permit YO-PRO-1 passage. Moreover, detectable uptake of the dye into the cells was not observed even in response to ten repeated 50 ns

pulses (data not shown). This finding is not surprising and somehow expected since we have confirmed previously that detectable uptake of the dye into the cells was not observed in response to a pulse that was three times longer (i.e., 150 ns pulse), unless cells were exposed to a large number of NEPs repeatedly at a high E-field intensity that causes significant cell swelling (Bagalkot et al. 2018).

From these results, we can conclude that VGCCs are responsible for the majority of $Ca^{2+}$ influx evoked by the NEP when the pulse duration is less than 11 ns. However, when the pulse duration is increased to 50 ns, not only are VGCCs responsible for the $Ca^{2+}$ influx, but there seems to be activation of another pathway for $Ca^{2+}$ influx that is still impermeable to YO-PRO-1.

## 3.3 External $Na^+$ dependency of $Ca^{2+}$ influx changes as pulse duration changes

### 3.3.1 With extracellular $Na^+$ replaced with $TMA^+$, the $Ca^{2+}$ responses of the cells exposed to 11 ns or longer became less dependent on external $Na^+$

$Na^+$ entry into chromaffin cells can cause depolarization of the membrane that opens up VGCCs (Lopez et al., 1995). Also, our group has previously found that applying a 5 ns unipolar pulse to the cell causes $Na^+$ influx that evokes activation of VGCCs. (Craviso et al., 2011). With this background, we wanted to investigate if the cells exposed to pulses 3, 5, 11, and 50 ns in duration without external $Na^+$ will show $Ca^{2+}$ influx via VGCCs. To achieve this goal, cells were exposed to NEPs in a range of 3 to 50 ns in duration in $Na^+$-free BSS, where the $Na^+$ ion was replaced with $TMA^+$.

As the representative $Ca^{2+}$ response traces show in Figure 3.17 and Figure 3.18, the response of the cells exposed to a 3 ns pulse delivered in the absence of $Na^{+}$ was almost completely gone except for just one cell that showed a very small and transient $Ca^{2+}$ response (Figure 3.17B). For the case of a 5 ns pulse was delivered in the absence of $Na^{+}$ (Figure 3.17D), only 3 cells out of 24 cells responded to the pulse and exhibited a small amplitude. While for an 11 ns pulse, $Ca^{2+}$ response was abolished in 42% of the cells, with the responding cells showing a significantly reduced change in fluorescence intensity (Figure 3.18B). Lastly, as shown in Figure 3.18D, for a 50 ns pulse duration, substituting $Na^{+}$ with $TMA^{+}$ did not have a significant effect on the number of cells that showed $Ca^{2+}$ responses although the $Ca^{2+}$ response amplitude was significantly attenuated relative to the control.

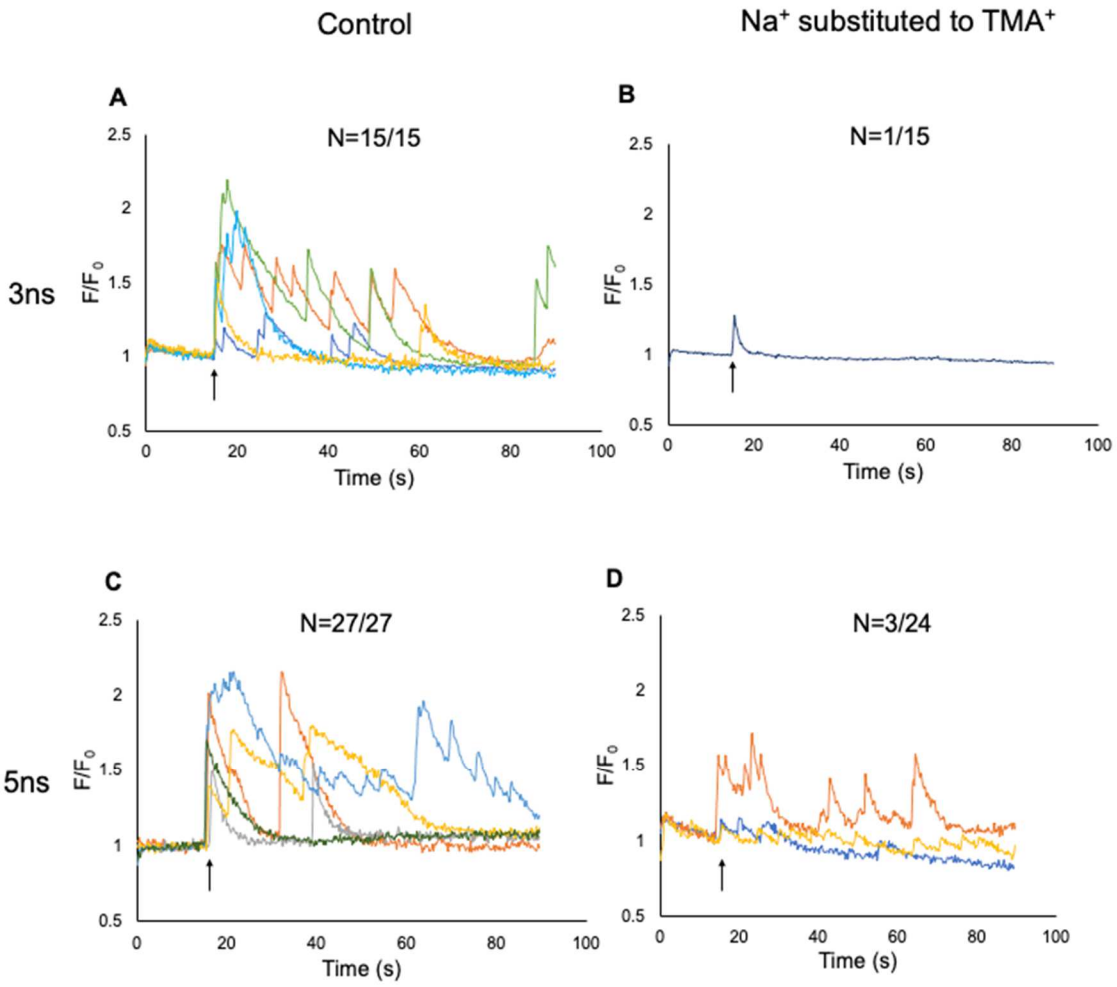


**Figure 3.17 Representative $Ca^{2+}$ traces of the cells exposed to a 3 and 5 ns pulse in the presence and absence of external $Na^+$, which was substituted with $TMA^+$.** The results show cells exposed to a 3 ns ((A) and (B)) and 5 ns ((C) and (D)) pulse in the presence and absence of external $Na^+$. The *n* on each plot represents the number of cells that responded to the pulse out of the total number of cells tested. Arrows indicate the time when the pulse was applied.

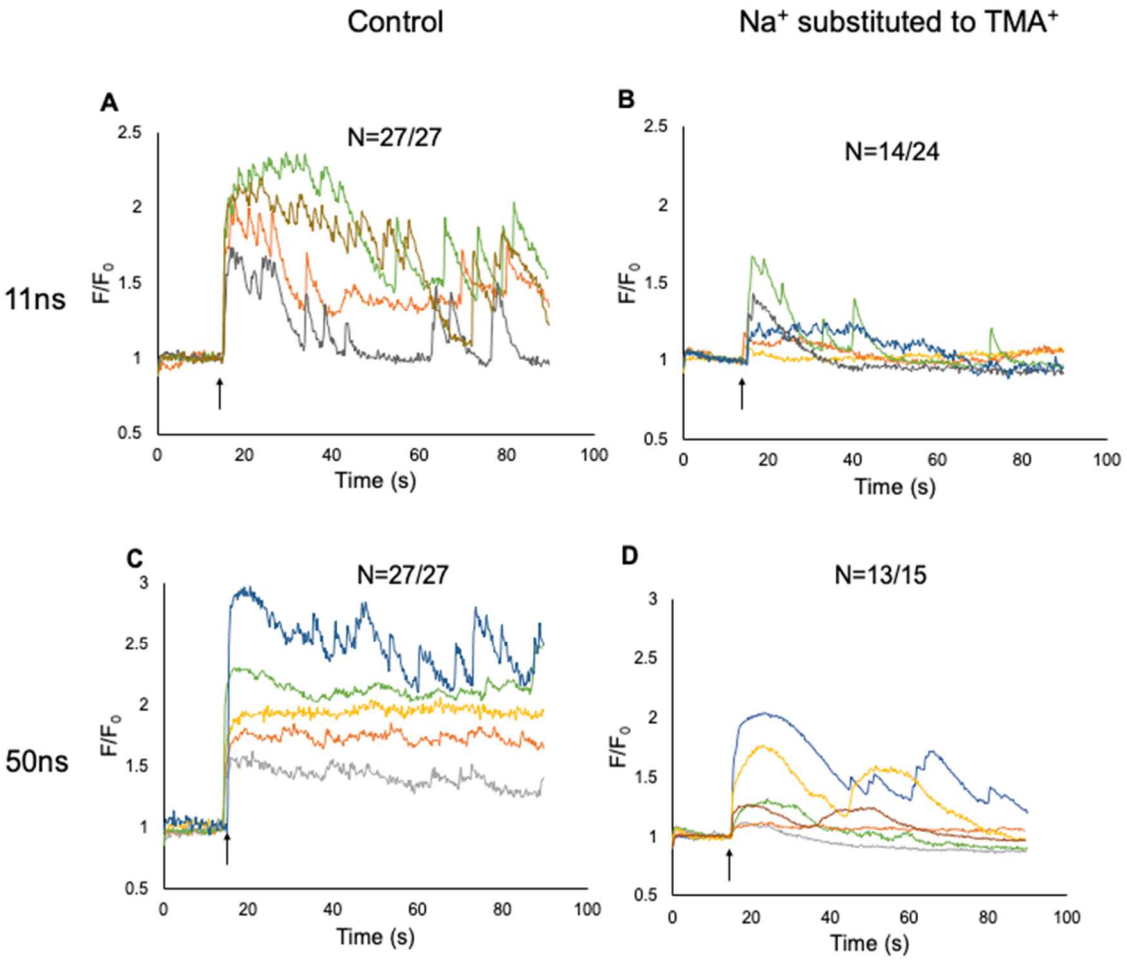


**Figure 3.18 Representative $Ca^{2+}$ responses traces of the cells exposed to a 11 and 50 ns pulse in the presence and absence of external $Na^+$, where it is substituted with $TMA^+$.** The results show cells exposed to a 11 ns ((A) and (B)) and 50 ns ((C) and (D)) pulse in the presence and absence of external $Na^+$. The *n* on each plot represents the number of cells that responded to the pulse out of the total number of cells tested. Arrows indicate the time when the pulse was applied.

Figure 3.19 shows the plots that combined averaged responses of the cells exposed to 3, 5, 11, and 50 ns under $Na^+$-free and versus control conditions. For the cells exposed to 3 and 5 ns duration of pulses, response amplitude for $Na^+$-free and control conditions was almost abolished (Figure 3.19A, B). The fluorescence intensity for Figure 3.19A is

1.05 ± 0.02 vs. 1.45 ± 0.07 for $Na^+$-free and control conditions, respectively. For Figure 3.19B, the fluorescence intensity was 1.07 ± 0.02 vs. 1.68 ± 0.05 for $Na^+$-free and control conditions, respectively. For the cells showing a significantly reduced change in fluorescence intensity with the application of an 11 ns duration pulse, it was 1.22 ± 0.05 vs. 1.97 ± 0.04 for $Na^+$-free and control conditions, respectively (Figure 3.19C). For a 50 ns pulse duration, substituting $Na^+$ with $TMA^+$ did not have a significant effect on abolishing the $Ca^{2+}$ responses for most of the cells, but the fluorescence intensity of $Na^+$-free condition was reduced to 1.30 ± 0.06 compared to 2.14 ± 0.06 for the control condition (Figure 3.19D). Taken together, these results indicate a dependence on extracellular $Na^+$ for cells exposed to pulses that were less than 11 ns in duration.

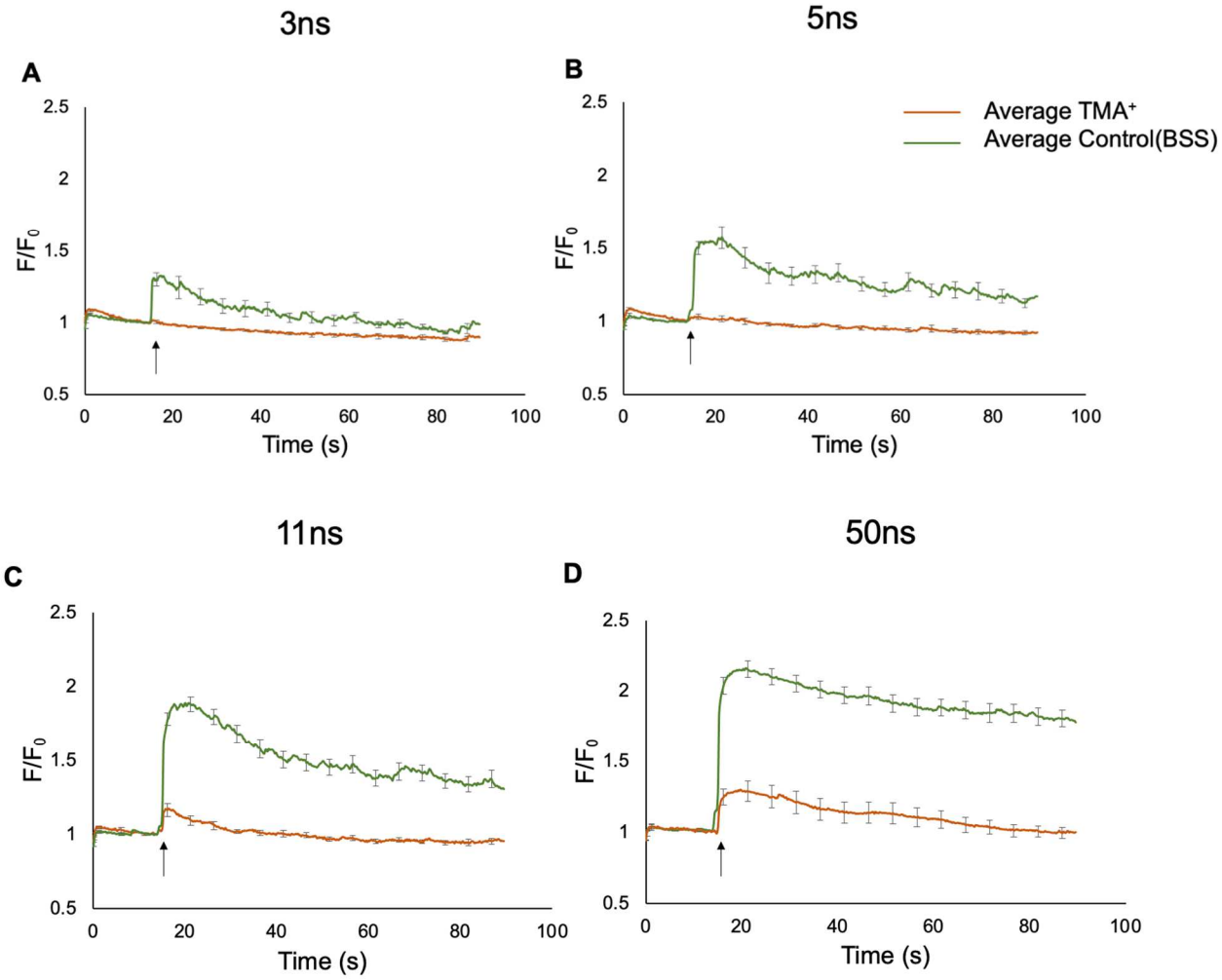


**Figure 3.19 Averaged effect of pulse duration on the $Ca^{2+}$ responses in cells exposed to a 3, 5, 11, and 50 ns pulse in the presence and absence of external $Na^{+}$.** Results are plotted as the averaged cell responses ± SEM for cells exposed to a (A) 3 ns, (B) 5 ns, (C) 11 ns, and (D) 50 ns pulse in the presence and absence of external $Na^{+}$; $n$ = 15 (BSS)/15 (TMA) for 3 ns, $n$ = 24 (BSS)/27 (TMA) for 5 ns, $n$ = 24 (BSS)/27 (TMA) for 11 ns, $n$ = 15 (BSS)/27 (TMA) for 50 ns. Arrows indicate the time when the pulse was applied.

Figure 3.20 summarizes the percentage of cells responding to the pulse under control (BSS), and $TMA^+$ added $Na^+$-free conditions. As the bar graph shows, the percentage of cells that respond to the pulse increases as pulse duration increases from 3 ns to 50 ns. Specifically, 0%, 13%, 58%, and 87% of the cells respond to the 3, 5, 11 and 50 ns pulse in the absence of extracellular $Na^+$, respectively.

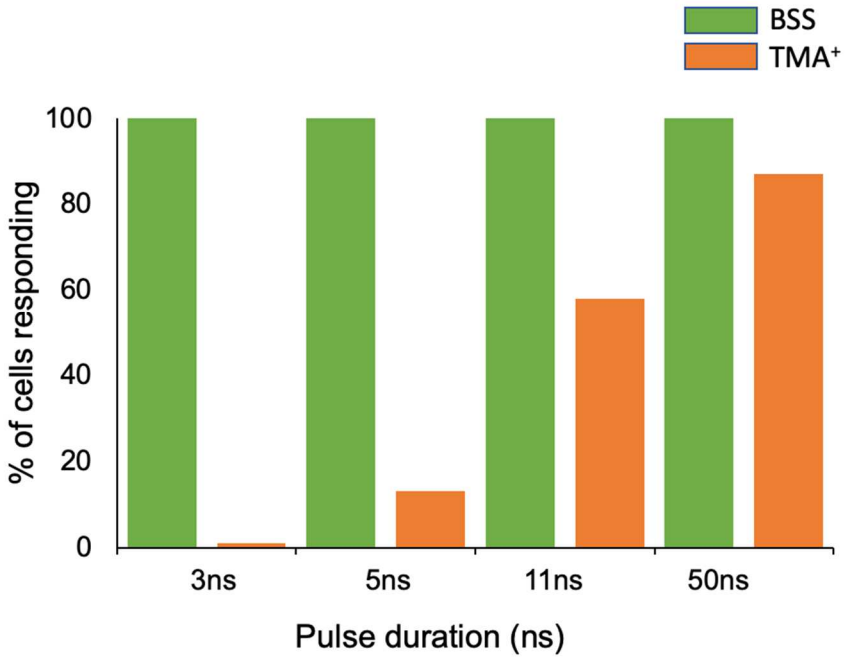


**Figure 3.20 Effect of pulse duration on the number of cells responding and the magnitude of the $Ca^{2+}$ response in cells exposed to NEPs in the presence and absence of external $Na^+$.** The plot shows the percentage of cells responding to the pulse in the presence of $TMA^+$ for each pulse duration.

Figure 3.21 summarizes the average $Ca^{2+}$ peaks for the different pulse durations under different experimental conditions. We only averaged those cells that exhibited a response to the pulse in the presence of $TMA^{+}$ to compare the fluorescence intensity with the control condition. It clearly shows that the magnitude of the increase in fluorescence intensity was significantly reduced without external $Na^{+}$ relative to the control. For 3 ns pulse, the peak amplitudes were 1.45 ± 0.07 vs. 1.05 ± 0.02; for a 5 ns pulse, peak amplitudes were 1.68 ± 0.05 vs. 1.28 ± 0.15; for a 11 ns pulse, peak amplitudes were 1.30 ± 0.06 vs. 1.97 ± 0.04; and for a 50 ns pulse, peak amplitudes were 1.34 ± 0.07 vs. 2.14 ± 0.06, for $Na^{+}$-free and control conditions, respectively.

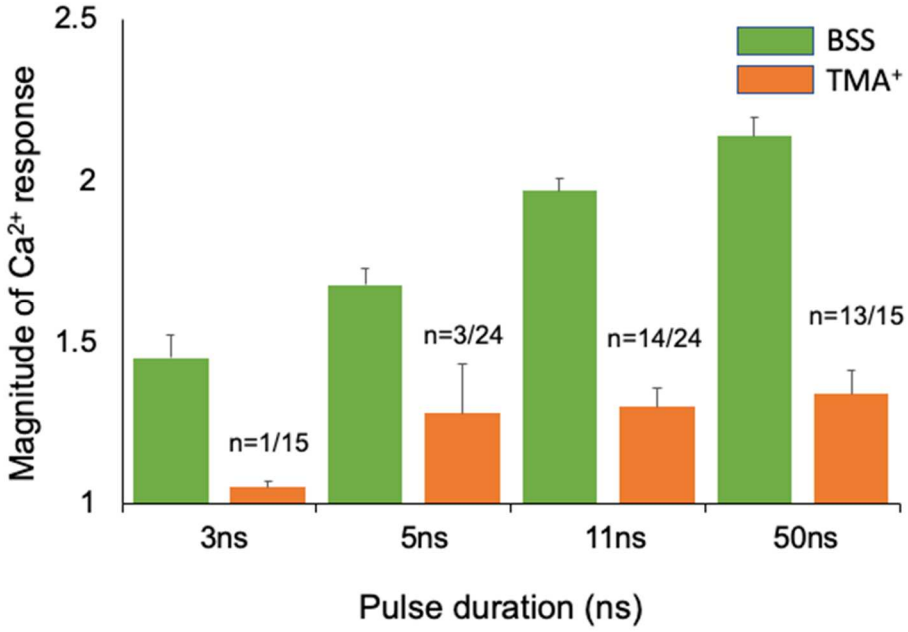


**Figure 3.21 Effect of pulse duration on the magnitude of the $Ca^{2+}$ response in cells exposed to NEPs in the presence and absence of external $Na^{+}$.** Shown is the magnitude of the $Ca^{2+}$ response as a function of pulse duration, both in the absence and presence of external $Na^{+}$. In each case, *n* represents the number of cells responding to the pulse out of the total number of cells tested for each pulse duration.

### 3.3.2 **Replacing extracellular $Na^+$ with $NMDG^+$, no $Ca^{2+}$ response was observed with 5 ns pulse applied, while $Ca^{2+}$ response was reduced but not totally abolished for a 11 ns pulse**

Similar results were obtained when external $Na^+$ was replaced with *N*-methyl-D-glucamine ($NMDG^+$). Specifically, there was no rise in $[Ca^{2+}]_i$ observed in response to a 5 ns pulse applied in the presence of $NMDG^+$ (Figure 3.22A, B), whereas applying an 11 ns pulse resulted in a significantly attenuated $Ca^{2+}$ response when $Na^+$ was substituted with $NMDG^+$ in the external solution (Figure 3.22C, D). In the case that a 5 ns pulse was delivered in the absence of $Na^+$ with the presence of $NMDG^+$, none of the 8 cells responded (Figure 3.19B), while for an 11 ns pulse, $Ca^{2+}$ response was abolished in 33% of the cells, with 67% of responding cells showing a significantly reduced change in fluorescence intensity (Figure 3. 20D).

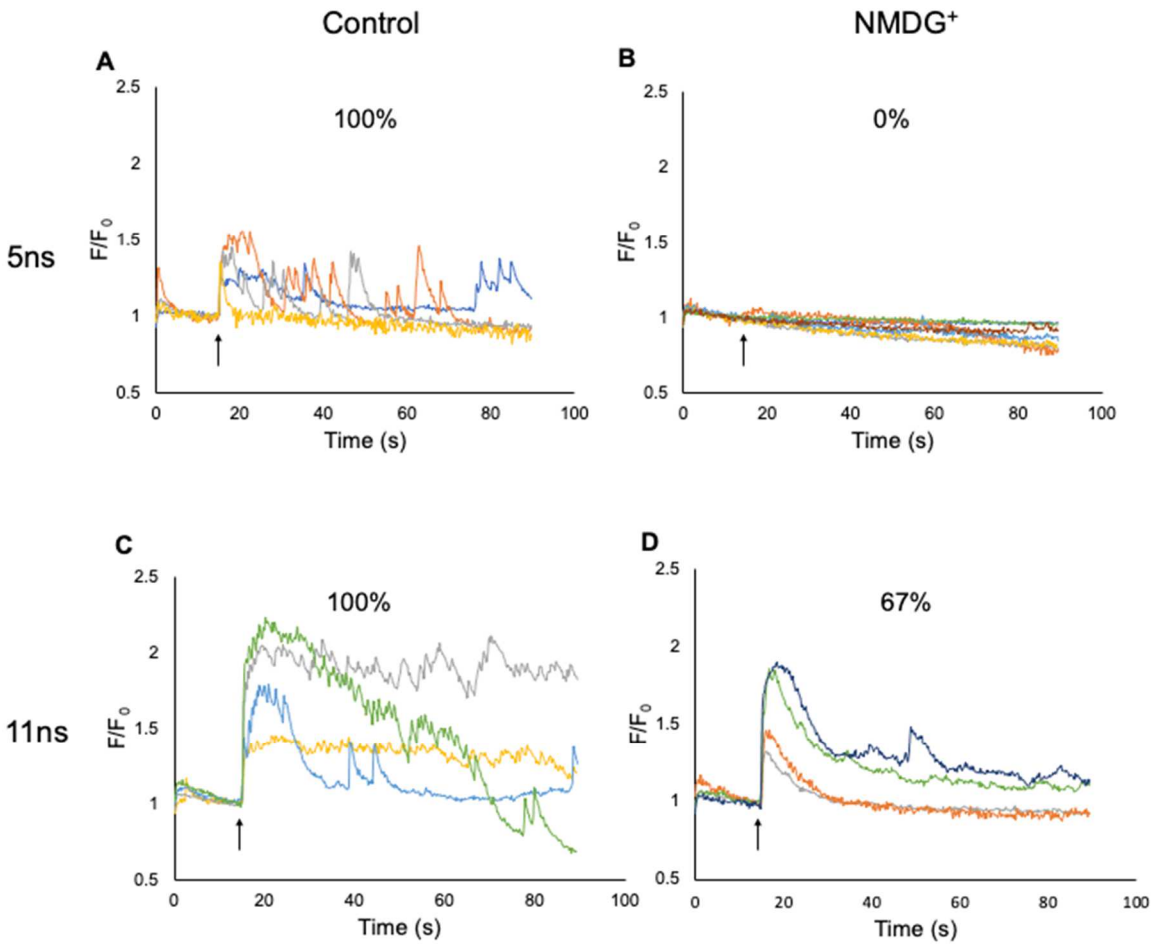


**Figure 3.22 Representative responses showing the Effect of pulse duration on the $Ca^{2+}$ responses in cells exposed to a 5 and 11 ns pulse in the presence and absence of external $Na^{+}$.** (A) and (B) shows representative traces for cells exposed to a 5 ns pulse ($n$ = 6 for control; 8 for $NMDG^{+}$). Figure (C) and (D) shows representative traces for cells exposed to an 11 ns pulse ($n$ = 6 for control; 9 for $NMDG^{+}$) applied at threshold E-field amplitude, respectively. Arrows indicate the time when the pulse was applied.

Compared to the result obtained by replacing external $Na^{+}$ with $TMA^{+}$, there was a noticeable difference in the rise of the amplitude of the $Ca^{2+}$ influx when an 11 ns duration pulse was applied. The $Ca^{2+}$ response peak was slightly higher in the $NMDG^{+}$-containing than in the $TMA^{+}$-containing solution when applied with 11 ns unipolar pulse (1.36 ± 0.1

vs. 1.22 ± 0.05 for $NMDG^+$ and $TMA^+$, respectively). This difference could potentially be due to the difference in the conductivity of the $NMDG^+$ solution compared to that of the $TMA^+$ solution and BSS (conductivities of the $NMDG^+$-containing, $TMA^+$-containing, and $Na^+$-containing solutions are: 11.3 ± 0.1 mS/cm, 14.9 ± 0.5 mS/cm, and 17.3 ± 0.2 mS/cm, respectively).

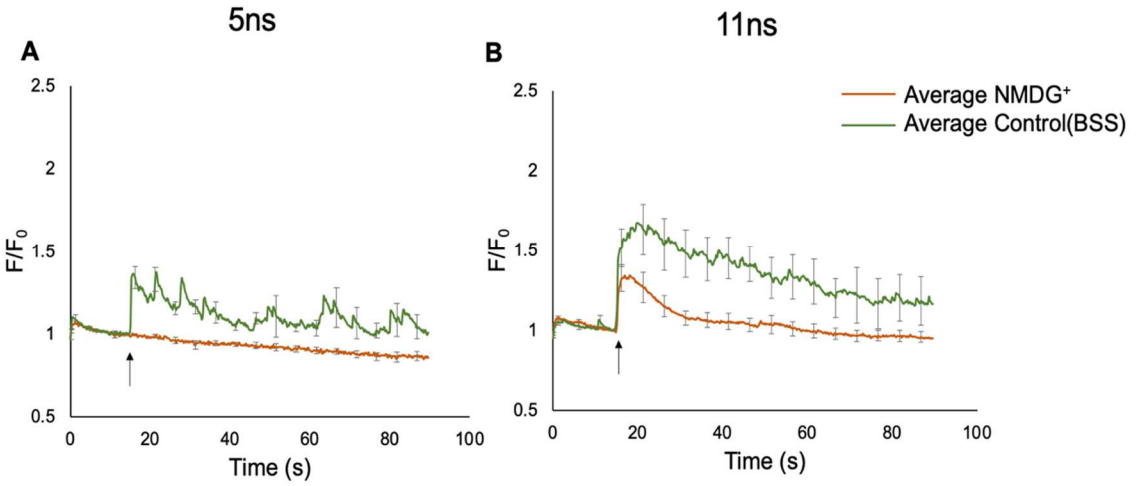


**Figure 3.23 Averaged Effect of pulse duration on the $Ca^{2+}$ responses in cells exposed to a 5 and 11 ns pulse in the presence and absence of external $Na^+$.** (A) and (B) represent averaged cells responses ± SD for cells exposed to a 5 ns pulse ($n$ = 6 for control; 8 for $NMDG^+$) and a 11 ns pulse ($n$ = 6 for control; 9 for $NMDG^+$) applied at threshold E-field amplitude, respectively. Arrows indicate the time when the pulse was applied.

Taken together, the results indicate that NEP-induced $Ca^{2+}$ influx is dependent on external $Na^+$ for pulses 3 and 5 ns in duration. When the pulse duration is increased to only 11 ns, $Ca^{2+}$ responses start to become less, though still significantly dependent, on external $Na^+$. This pulse duration of 11 ns also coincides with the pulse duration at which $Ca^{2+}$ influx occurs not only via VGCCs but also through another pathway independent of VGCCs.

### 3.4 Pretreating cells with TTX had no effect on the $Ca^{2+}$ responses for 5, 11 and 50 ns pulses, meaning that VGSCs were not involved in the response of chromaffin cells to NEPs

From our previous studies, we have found that the voltage-gated sodium channel activity is not responsible for $Na^+$ entry into the cells (Craviso et al., 2010), since TTX failed to block the pulse-induced rise in $[Ca^{2+}]_i$ in cells exposed to a single 5 ns pulse. Thus, we wanted to investigate the possibility of VGSCs' involvement in the $Ca^{2+}$ response with pulses ranging from 5 to 50 ns in duration. Cells were treated with $Na^+$ channel blocker, TTX with the concentration of 10 μM, incubated for 20 min at room temperature, and 5, 11, and 50 ns unipolar pulses were applied to see the effect of the toxin on the $Ca^{2+}$ responses. As a result, representative $Ca^{2+}$ response traces were obtained. As shown in Figure 3.24, no significant difference was observed in the number of cells responding nor the magnitude of the cell response in the presence of TTX. These results show that pretreating cells with TTX had no effect on the $Ca^{2+}$ responses for all pulse durations, leading us to conclude that VGSCs are not involved in the response of chromaffin cells to NEPs at any pulse duration.

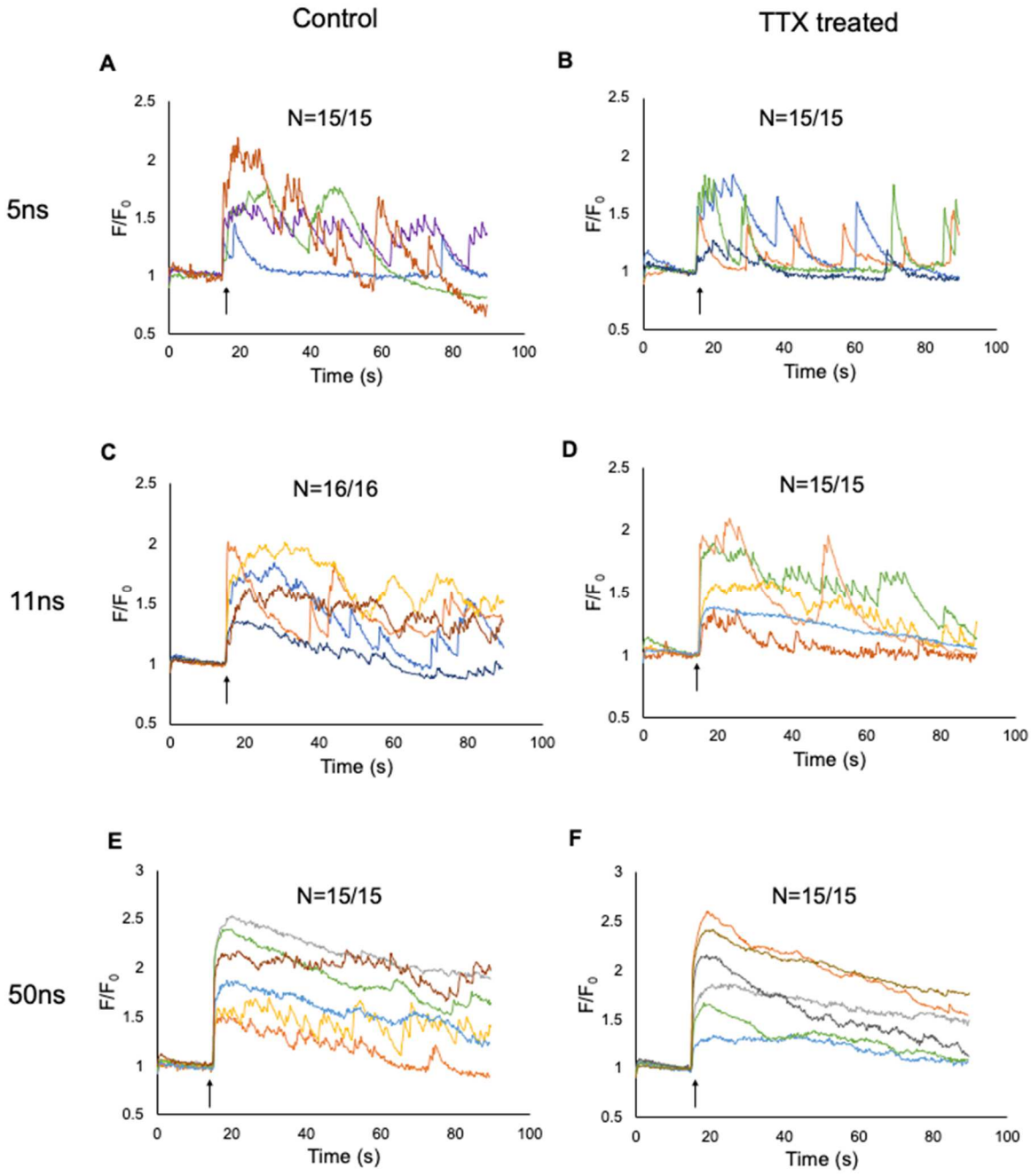


**Figure 3.24 Representative $Ca^{2+}$ responses in cells showing the effect of blocking TTX-sensitive VGSCs on the increase in $[Ca^{2+}]_i$ evoked by 5, 11, and 50 ns pulses.** Results are plotted as the representative $Ca^{2+}$ responses in cells exposed to an (A) and (B) 5 ns, (C) and (D) 11 ns, and (E) and (F) 50 ns pulse in regular BSS, or TTX containing BSS, $n$ = 15 (BSS)/15 (TTX) for 5 ns, $n$ = 16 (BSS)/15 (TTX) for 11 ns, $n$ = 15 (BSS)/15 (TTX) for 50 ns. Arrows indicate the time when the pulse was applied.

The averaged cell responses ± SEM for cells exposed to a (A) 5 ns, (B) 11 ns, and (C) 50 ns pulse in regular BSS or TTX containing BSS are shown in Figure 3.22. The magnitude of the increase in fluorescence intensity did not show a reduction with TTX treated condition compared to the control. The peak amplitude for each condition according to the presence and the absence of TTX was very minor. The mean $Ca^{2+}$ amplitudes were 1.45 ± 0.06 ($n$ = 15) vs. 1.41 ± 0.06 ($n$ = 15) (5 ns pulse); 1.46 ± 0.11 ($n$ = 15) vs. 1.54 ± 0.05 ($n$ = 15) (11 ns pulse); and 1.86 ± 0.12 ($n$ = 15) vs. 1.90 ± 0.07 ($n$ = 15) (50 ns pulse), for TTX treated and control conditions, respectively.

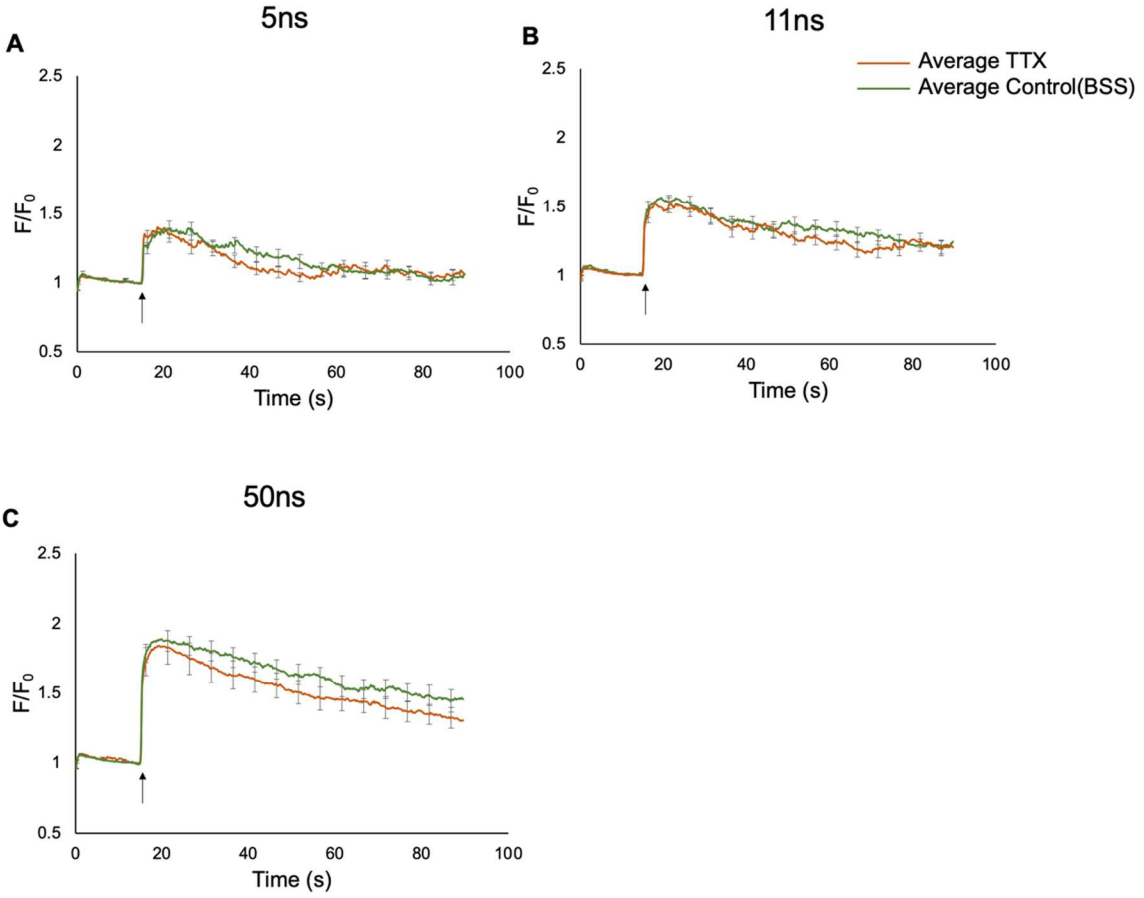


**Figure 3.25 Average $Ca^{2+}$ responses in cells showing the effect of blocking TTX-sensitive VGSCs on the increase in $[Ca^{2+}]_i$ evoked by 5, 11, and 50 ns pulses.** Results are plotted as the averaged cell responses ± SEM for cells exposed to a (A) 5 ns, (B) 11 ns, and (C) 50 ns pulse in regular BSS, or TTX containing BSS. Arrows indicate the time when the pulse was applied.

## 3.5 Using an 11 ns bipolar pulse, all $Ca^{2+}$ influx occurred via VGCCs

After characterizing the $Ca^{2+}$ responses to unipolar pulse exposures ranging from 3 to 50 ns in duration and determining that $Ca^{2+}$ entry occurred via an additional pathway that does not involve VGCCs when the pulse duration increased to 11 ns, we next

investigated whether applying a bipolar pulse can eliminate/reduce the additional pathway for $Ca^{2+}$ entry into cells.

Thus, we performed an experiment in which cells were exposed to a 11ns bipolar pulse in the presence and absence of VGCC blockers. Figure 3.26A shows representative $Ca^{2+}$ responses in cells exposed to 11 ns in the absence of VGCC blockers. The plot shows the cells that responded to the bipolar pulse. Figure 3.26B shows that all the cells ($n$ = 18) did not respond to the pulse in the presence of VGCC blockers.

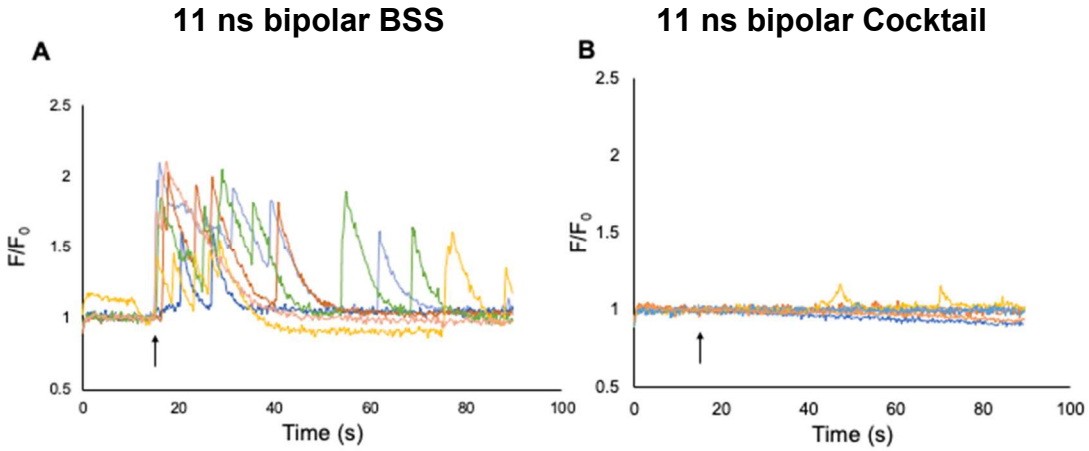


**Figure 3.26 Representative $Ca^{2+}$ responses in cells exposed to a single 11 ns symmetrical bipolar pulse in the presence and absence of the cocktail.** (A) shows representative $Ca^{2+}$ responses in cells exposed to 11 ns bipolar pulse with the BSS, and (B) shows representative $Ca^{2+}$ responses in cells exposed to 11 ns bipolar pulse with the presence of a cocktail of VGCC blockers. Arrows indicate the time when the pulse was applied.

The averaged cell responses ± SEM for cells exposed to a 11 ns unipolar and 11 ns bipolar in regular BSS or in the presence of a cocktail of VGCC, are shown in Figure 3.27 The magnitude of the increase in fluorescence intensity showed a clear reduction in the presence of the cocktail of VGCC inhibitors. The magnitude of the increase in fluorescence

intensity was 1.19 ± 0.02 vs. 1.97 ± 0.04 for a 11 ns unipolar pulse (Figure 3.27A) and 1.03 ± 0.01 vs. 1.34 ± 0.10 for a 11 ns bipolar pulse, (Figure 3.27B) both for VGCC blockers treated and control conditions, respectively.

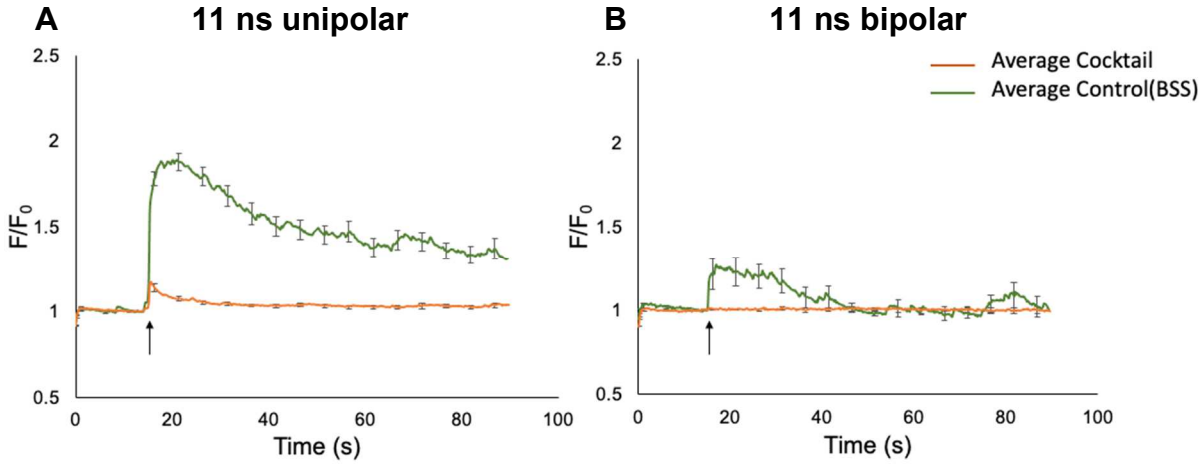


**Figure 3.27 Averaged $Ca^{2+}$ responses in cells exposed to a single 11 ns symmetrical bipolar pulse in the presence and absence of the cocktail.** Averaged cells responses ± SEM for cells exposed to a (A) 11 ns unipolar pulse ($n$ = 8 for control; 15 for the cocktail), and (B) 11 ns bipolar pulse ($n$ = 8 for control; 18 for the cocktail). Arrows indicate the time when the pulse was applied.

These results are summarized in a bar graph in Figure 3.28 and shown together with the 11 ns unipolar conditions. Also shown on the plot is the number of the cells that responded out of the total number of cells tested under each condition. The averaged magnitude of the $Ca^{2+}$ responses represents that of the cells that showed a response to the pulse.

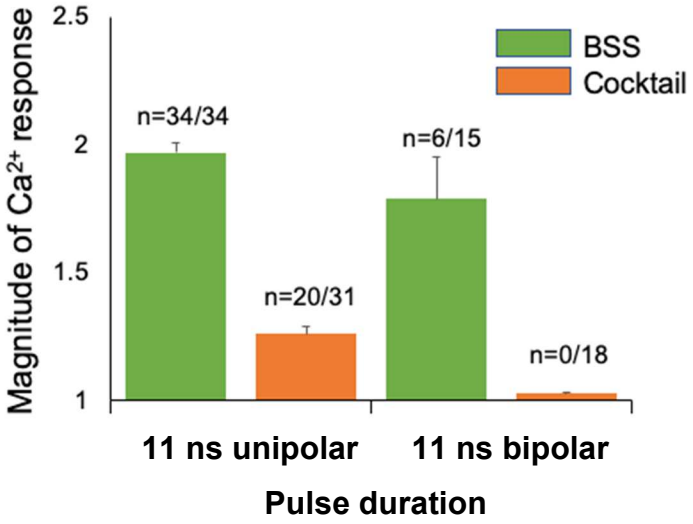


**Figure 3.28 Summary of $Ca^{2+}$ responses in cells exposed to a single 11 ns symmetrical bipolar pulse and 11 ns unipolar pulse, under control and VGCC-blocked conditions.** The bar represents the averaged magnitude of the $Ca^{2+}$ responses ± SEM in cells that responded to the pulse under each condition.

The results show that VGCCs are fully blocked when a bipolar pulse is applied in the presence of the cocktail. This result indicates that all the $Ca^{2+}$ influx that occurred with 11ns bipolar pulse happened via VGCCs.

# Chapter 4. CONCLUSION AND FUTURE WORK

## Conclusion

In this project, the effect of increasing pulse duration on the $Ca^{2+}$ responses in adrenal chromaffin cells was investigated and the pulse duration at which $Ca^{2+}$ influx started to involve a non-VGCC pathway was identified. In a study by Casciola et al. (2017) applying 12 ns pulses to a frog sciatic nerve, no damage was observed when 6000 12 ns pulses were applied. In the case of chromaffin cells, pulse duration appears to play a significant role as increasing the pulse duration from 5 to 150 ns causes an additional, non-VGCC pathway that allows $Ca^{2+}$ entry into cells. This means that different excitable systems react differently to NEPs. Since the ultimate goal is to use NEPs for noninvasive neuromodulation, it is imperative to determine the pulse duration(s) that causes $Ca^{2+}$ responses to mimic those evoked by the physiological stimulus, i.e., in which $Ca^{2+}$ entry would involve only VGCCs.

Thus, first, we characterized the nature of the $Ca^{2+}$ responses (i.e., transient vs longer-lived) at each pulse duration. The $Ca^{2+}$ responses elicited by 3 and 5 ns pulses exhibited transient $[Ca^{2+}]_i$ response in the majority of the cells (88% and 74%, respectively), whereas increasing the pulse duration to 11 and 50 ns caused the majority of the cells to show longer-lived responses in $[Ca^{2+}]_i$ (77% and 100% of the cells, respectively). $[Ca^{2+}]_i$ rise for 11 and 50 ns was found to be solely dependent on extracellular $Ca^{2+}$. In addition, by 11 ns, the activation of the non-VGCC pathway for $Ca^{2+}$ influx was observed, in the absence of YO-PRO-1 uptake. The cocktail of VGCC blockers not being able to block the majority of the responses by 50 ns pulses is consistent with the previous

results using 150 ns pulse (Bagalkot et al. 2018). We also studied the role of $Na^+$ in the $Ca^{2+}$ responses and found that $Ca^{2+}$ influx became less dependent on external $Na^+$ when the pulse duration was increased beyond 11 ns. Yet, the pathway for $Na^+$ entry into cells remains to be determined as it does not occur via VGSCs.

Lastly, we investigated the effect of a 11 ns bipolar on the $Ca^{2+}$ responses. In looking at the involvement of VGCCs, we found that a 11 ns bipolar pulse causes $Ca^{2+}$ influx solely via VGCCs.

**Future work**

A potential reason for the longer-lived $Ca^{2+}$ responses observed with increased pulse duration could be that NEPs are affecting $Ca^{2+}$ uptake into the mitochondria, a structure that has been previously reported to be affected by NEPs (Napotnik et al., 2011). In chromaffin cells, mitochondria are the main organelles involved in the rapid clearing of intracellular $Ca^{2+}$ when $Ca^{2+}$ influx through VGCCs occurs. Disruption of mitochondrial membrane potential has been shown to delay $Ca^{2+}$ clearance (García et al., 2006; García-Sancho and Verkhratsky, 2008). Our group has recently explored whether a 5 ns pulse affects mitochondrial membrane potential using a fluorescent mitochondrial membrane potential dye. We found that a single 5 ns pulse applied at threshold E-field does not affect mitochondrial membrane potential (Ruby, 2019). However, longer duration NEP's effect on the mitochondria remains to be further explored.

In addition, a potential explanation for the failure of the cocktail of VGCC inhibitors to fully block $Ca^{2+}$ influx when the pulse duration increases beyond 11 ns could

be an increase in the length of time the membrane remains depolarized. This could mean that VGCCs remain open for longer periods of time and possibly become less amenable to being blocked by VGCC inhibitors. Another possibility could be that as pulse duration increases, the pulse has a direct effect on VGCCs, as reported in Nesin et al.(2012) where the authors found that longer duration pulses (300 and 600 ns) exerted a prolonged inhibitory effect on voltage-gated $Na^+$ and $Ca^{2+}$ channels in GH3 cells, NG108 cells and adrenal chromaffin cells (Nesin et al., 2012).

Another possibility that the VGCC inhibitors could not fully block the $Ca^{2+}$ influx with an 11 or longer-duration pulse applied is that there can be $Ca^{2+}$ influx occurring via non-VGCCs that are permeable to $Ca^{2+}$. Cheek and Thorn (2006) reported the presence of a non-selective cation channel in chromaffin cells that is permeable to both monovalent ($Na^+$) and divalent ($Ca^{2+}$) cations (Cheek and Thorn, 2006). We previously reported that blocking this non-selective cation channel with $La^{3+}$ did not affect the NEP-evoked $Ca^{2+}$ influx in cells exposed to a single 5 ns pulse (Craviso et al., 2010). This indicates that this channel does not appear to play a role in $Ca^{2+}$ entry into cells for the shortest pulse duration. However, for the longer duration pulses it is yet to be determined. Furthermore, Momboisse et al. (2014) reported that bovine adrenal chromaffin cells express Pannexin 1 channels at their plasma membrane that are permeable to $Ca^{2+}$ (Momboisse et al., 2014). The effect of blocking these channels with probenecid is currently under investigation.

Lastly, we show that $Na^+$ influx does not occur via VGSCs since TTX failed to block the pulse-induced $Ca^{2+}$ response. In addition, even as pulse duration increases beyond 11 ns, VGSCs are still not responsible for $Na^+$ entry into cells. These findings are strikingly

different from the study that reported in frog sciatic nerve, where the authors reported that nerve excitation by 12 ns occurs because of VGSC activation (Casciola et al., 2017). Using whole-cell patch clamp electrophysiology, we recently found that a large fraction of the NEP-induced membrane current evoked by a 5 ns pulse may be carried by both TRPC4/5 channels and the NALCN channel expressed in chromaffin cells (Yang et al., 2022). Whether these channels are also involved in $Na^+$ entry for pulse durations longer than 5 ns is still to be investigated.

This work is significant because it shows the exquisite sensitivity of an excitable neural-type cell to NEPs, that differ by only tens of nanosecond in duration. This study provides essential information to be used when developing NEP-based technologies for neuromodulation.

# REFERENCES


Bagalkot TR, Leblanc N, Craviso GL. Stimulation or cancellation of Ca2+ influx by bipolar nanosecond pulsed electric fields in adrenal chromaffin cells can be achieved by tuning pulse waveform. Sci. Rep. 9:11545, 2019.

Bagalkot TR, Terhune RC, Leblanc N, Craviso GL. Different membrane pathways mediate $Ca^{2+}$ influx in adrenal chromaffin cells exposed to 150-400 ns electric pulses. Biomed. Res. Int. 9046891, 2018.

Casciola, M., Xiao, S., Apollonio, F., Paffi, A., Liberti, M., Muratori, C., & Pakhomov, A. G. (2019). Cancellation of nerve excitation by the reversal of nanosecond stimulus polarity and its relevance to the gating time of sodium channels. *Cellular and Molecular Life Sciences*, *76*(22), 4539-4550.

Casciola M, Xiao S, Pakhomov AG. Damage-free peripheral nerve stimulation by 12-ns pulsed electric field. Sci Rep. 2017;7(1):10453. Epub 2017/09/07. pmid:28874684; PubMed Central PMCID: PMC5585227

Cheek, T. R., & Thorn, P. (2006). A constitutively active nonselective cation conductance underlies resting Ca2+ influx and secretion in bovine adrenal chromaffin cells. *Cell Calcium*, *40*(3), 309-318.

Craviso, G. L. (2004). Generation of functionally competent single bovine adrenal chromaffin cells from cell aggregates using the neutral protease dispase. *Journal of neuroscience methods*, *137*(2), 275-281.

Craviso, G. L., Choe, S., Chatterjee, P., Chatterjee, I., & Vernier, P. T. (2010). Nanosecond electric pulses: a novel stimulus for triggering Ca2+ influx into chromaffin cells via voltage-gated Ca2+ channels. *Cellular and molecular neurobiology*, *30*(8), 1259-1265.

Craviso, G. L., Choe, S., Chatterjee, I., & Vernier, P. T. (2012). Modulation of intracellular Ca2+ levels in chromaffin cells by nanoelectropulses. *Bioelectrochemistry*, *87*, 244-252.

Dunlop, K., Hanlon, C. A., & Downar, J. (2017). Noninvasive brain stimulation treatments for addiction and major depression. *Annals of the New York Academy of Sciences*, *1394*(1), 31-54.

Gianulis, E. C., Casciola, M., Zhou, C., Yang, E., Xiao, S., & Pakhomov, A. G. (2019). Selective distant electrostimulation by synchronized bipolar nanosecond pulses. Scientific reports, 9(1), 1-10.

Ibey, B. L., Ullery, J. C., Pakhomova, O. N., Roth, C. C., Semenov, I., Beier, H. T., ... & Pakhomov, A. G. (2014). Bipolar nanosecond electric pulses are less efficient at electropermeabilization and killing cells than monopolar pulses. *Biochemical and biophysical research communications*, *443*(2), 568-573.

Jiang, N., & Cooper, B. Y. (2011). Frequency□dependent interaction of ultrashort E□ fields with nociceptor membranes and proteins. *Bioelectromagnetics*, *32*(2), 148-163.

Kim, V., Semenov, I., Kiester, A. S., Keppler, M. A., Ibey, B. L., Bixler, J. N., & Pakhomov, A. G. (2022). Action spectra and mechanisms of (in) efficiency of bipolar electric pulses at electroporation. *Bioelectrochemistry*, 108319.

Nizard, J., Lefaucheur, J. P., Helbert, M., de Chauvigny, E. & Nguyen, J. P. Non-invasive stimulation therapies for the treatment of refractory pain. *Discovery medicine* **14**, 21–31 (2012).

Pakhomov, A. G., & Pakhomova, O. N. (2020). The interplay of excitation and electroporation in nanosecond pulse stimulation. *Bioelectrochemistry*, *136*, 107598.

Pakhomov, A. G., Semenov, I., Xiao, S., Pakhomova, O. N., Gregory, B., Schoenbach, K. H., ... & Ibey, B. L. (2014). Cancellation of cellular responses to nanoelectroporation by reversing the stimulus polarity. *Cellular and molecular life sciences*, *71*(22), 4431-4441.

Pakhomov, A. G., Shevin, R., White, J. A., Kolb, J. F., Pakhomova, O. N., Joshi, R. P., & Schoenbach, K. H. (2007). Membrane permeabilization and cell damage by ultrashort electric field shocks. *Archives of biochemistry and biophysics*, *465*(1), 109-118.

Perlmutter JS, Mink JW. Deep brain stimulation. *Annual Review of Neuroscience.* 2006;29:229-257.

Petrella, R. A., Schoenbach, K. H., & Xiao, S. (2016). A dielectric rod antenna for picosecond pulse stimulation of neurological tissue. *IEEE Transactions on Plasma Science*, *44*(4), 708-714.

Rodriguez-Oroz M, Zamarbide I, Guridi J, Palmero M, Obeso J. Efficacy of deep brain stimulation of the subthalamic nucleus in Parkinson's disease 4 years after surgery: double blind and open label evaluation. *Journal of Neurology, Neurosurgery & Psychiatry.* 2004;75(10):1382-1385.

Roth, C. C., Tolstykh, G. P., Payne, J. A., Kuipers, M. A., Thompson, G. L., DeSilva, M. N., & Ibey, B. L. (2013). Nanosecond pulsed electric field thresholds for nanopore formation in neural cells. *Journal of biomedical optics*, *18*(3), 035005.

Semenov, I., Xiao, S., & Pakhomov, A. G. (2013). Primary pathways of intracellular Ca2+ mobilization by nanosecond pulsed electric field. *Biochimica et Biophysica Acta (BBA)-Biomembranes*, *1828*(3), 981-989.

Schoenbach, K. H., Pakhomov, A. G., Semenov, I., Xiao, S., Pakhomova, O. N., & Ibey, B. L. (2015). Ion transport into cells exposed to monopolar and bipolar nanosecond pulses. *Bioelectrochemistry*, *103*, 44-51.

Sorimachi, M., Nishimura, S., & Yamagami, K. (1994). Inability of Ca2+ influx through nicotinic ACh receptor channels to stimulate catecholamine secretion in bovine adrenal chromaffin cells: studies with fura-2 and SBFI microfluorometry. *The Japanese Journal of Physiology*, *44*(4), 343-356.

Vernier, P. T., Sun, Y., Chen, M. T., Gundersen, M. A., & Craviso, G. L. (2008). Nanosecond electric pulse-induced calcium entry into chromaffin cells. *Bioelectrochemistry*, *73*(1), 1-4.

Yang, L., Pierce, S., Chatterjee, I., Craviso, G. L., & Leblanc, N. (2020). Paradoxical effects on voltage-gated Na+ conductance in adrenal chromaffin cells by twin vs single high intensity nanosecond electric pulses. *PloS one*, *15*(6), e0234114.

Zaklit, J., Cabrera, A., Shaw, A., Aoun, R., Vernier, P. T., Leblanc, N., & Craviso, G. L. (2021). 5 ns electric pulses induce Ca2+-dependent exocytotic release of catecholamine from adrenal chromaffin cells. *Bioelectrochemistry*, *140*, 107830.

Zaklit, J., Craviso, G. L., Leblanc, N., Vernier, P. T., & Sözer, E. B. (2021). 2-ns Electrostimulation of Ca2+ Influx into Chromaffin Cells: Rapid Modulation by Field Reversal. *Biophysical journal*, *120*(3), 556-567.

Zaklit, J., Craviso, G. L., Leblanc, N., Yang, L., Vernier, P. T., & Chatterjee, I. (2017). Adrenal chromaffin cells exposed to 5-ns pulses require higher electric fields to porate intracellular membranes than the plasma membrane: an experimental and modeling study. *The Journal of Membrane Biology*, *250*(5), 535-552.